2023-06-26

Characterizing Dust from National Wind Erosion Research Network Sites Using Strontium Isotopes, Major and Trace Element Chemistry, and Mineralogy

Abby L. Mangum
Brigham Young University

Characterizing Dust from National Wind Erosion Research Network Sites Using Strontium Isotopes, Major and Trace Element Chemistry, and Mineralogy

Abby L. Mangum

A thesis submitted to the faculty of
Brigham Young University
in partial fulfillment of the requirements for the degree of

Master of Science

Gregory T. Carling, Chair
Stephen T. Nelson
Zachary Aanderud
Joshua LeMonte

Department of Geological Sciences

Brigham Young University

ABSTRACT

Characterizing Dust from National Wind Erosion Research Network Sites Using Strontium Isotopes, Major and Trace Element Chemistry, and Mineralogy

Abby L. Mangum
Department of Geological Sciences, BYU
Master of Science

The frequency of dust storms is increasing globally yet it is often difficult to determine dust sources in mixed events. Dust events may negatively impact human health, but the composition of major dust sources is not well characterized in arid regions globally. In the western US, the National Wind Erosion Research Network (NWERN) has various sites evaluating seasonal dust emissions to quantify dust fluxes. We used existing dust samples to characterize the isotopic, chemical, and mineralogical composition of dust over multiple seasons from ten representative NWERN sites and compared with land use, vegetation, and surficial geology. Our results show variability in dust chemistry across the ten sites primarily related to differences in surficial geology (local bedrock and sediment) with other factors playing a minor role. In some cases, seasonal vegetation and wind direction played a role in controlling dust composition. For example, the El Reno site showed seasonal differences in mineralogy related to carbonate precipitation and dissolution in the soil during wet summers and dry winters. The Holloman Air Force Base (HAFB) site had distinct seasonal changes in dust chemistry with spikes in Na, Mg, Ca, Ni, and Sr during the spring months possibly related to changes in wind direction and inputs from neighboring White Sands National Park. The Lordsburg Playa site had distinct chemistry relative to other sites with high concentrations of Li, Na, Ca, and Sr due to the prevalence of evaporite minerals. Mineralogy results show the presence of quartz, phyllosilicates, and feldspar minerals at each of the NWERN sites with HAFB also containing calcium sulfate and iron oxide minerals. The $^{87}Sr/^{86}Sr$ results showed lower ratios correlating with younger bedrock (e.g., ~0.7075 at the Red Hills site surrounded by Miocene volcanic rocks), but some of the sites with recent surficial sediments had higher ratios (e.g., ~0.714 at the CPER site with Tertiary sediments). By creating a library of isotopic, chemical, and mineralogical data for dust sources across the western US, our dataset has implications for identifying characteristics that may be used for tracking dust sources.

Keywords: dust chemistry, western US, dust, dust emissions, dust source, strontium isotopes, mineralogy, trace and major element chemistry

ACKNOWLEDGMENTS

Without the help of the following people, I would not be where I am today. I am so grateful for my committee and their guidance with my project. A special thanks to Dr. Steve Nelson for helping me prep and interpret so many XRD results. Thank you, Dr. Zach Aanderud, for letting me use the NWERN samples and to collaborate with your graduate student, Detiare Leifi. I'm excited to combine our data and write a paper together. I would especially like to thank my advisor Dr. Greg Carling for his kindness and friendship throughout graduate school. Thank you for taking me on with little to no geochemistry background and being an encouraging, guiding hand the whole way through.

A special thank you to Dr. Nick Webb and all the researchers at NWERN for collaborating with me and allowing me to use their dust samples for my thesis project. I am so honored to have been a part of your work and research.

A sincere thank you to Dr. Landon Burgener for helping me interpret my strontium isotope results and explore various interpolation methods in ArcGIS Pro. Thank you Alyssa Thompson and Dr. Barry Bickmore for developing an app on MATLAB to run a PCA and letting me use it! You saved me hours of frustration and coding.

I am also so grateful for the various friendships that have sustained me through school and the lifelong friendships I have made with the other graduate students. A big thank you to my parents and siblings as well for supporting me through all the ups and downs I have been through these last couple of years!

Finally, I am thankful for my Heavenly Father and the countless blessings I've seen throughout this process. I feel so blessed to have studied geology here at BYU, both for my undergraduate and graduate degrees. I have had incredible experiences traveling all over the world and learning to appreciate this Earth we live on.

TABLE OF CONTENTS

LIST OF FIGURES

LIST OF TABLES

1. INTRODUCTION

Dust events originate from a variety of sources in arid regions, but information about the composition of dust sources is lacking, making it difficult to track the source of dust events. A compilation of novel fingerprints is needed to identify dust sources to make it possible to identify key dust sources. Dust fingerprints may include isotopic tracers (Nakano et al., 2004; Négrel and Petelet-Giraud, 2005), geochemical tracers (Guinoiseau et al., 2022), mineralogy (Chen and Li, 2011; Menéndez et al., 2014), and microbes (Abed et al., 2012).

Dust emissions are increasing globally from a variety of factors, which may change seasonally or over longer time periods. These include changes in vegetation cover, precipitation, wind velocity, and soil moisture (Wanquan et al., 2004). Dust production is diverse across Earth's surface, and source regions occur in a variety of environments and land use types (Prospero et al., 2002). In addition to playas, open land, grazing fields, unpaved roads, and so forth are also important sources of dust (Middleton and Goudie, 2001). Increased human activity, such as agriculture and livestock grazing, in the American Southwest and the Colorado Plateau during the past several decades has been correlated with greater dust production and deposition and has been identified on mountain snowpacks on both seasonal to annual timescales (Neff et al., 2008; Painter et al., 2007; Reynolds et al., 2001).

Dust composition and particle size can have a negative effect on its surroundings. Mineral dust emitted from playas specifically has been shown to have a variety of potentially harmful effects to the environment and human health (Goodman et al., 2019b). This dust can cause diseases such as asthma, pneumonia, and valley fever in humans (Derbyshire, 2007; Kumar and Rajkumar, 2014; Pope et al., 1991), increase the frequency and intensity of harmful algal blooms in lakes (Brahney et al., 2015; Zhang, 1994), cause earlier snowmelt and decreased

runoff from mountain snowpack (Painter et al., 2010), and carry many organisms and metals that affect air quality and water resources (Carling et al., 2012; Dastrup, 2016; Kellogg and Griffin, 2006; McTainsh and Strong, 2007).

Dust sources can be identified by understanding the geochemical composition of dust. Geochemical fingerprints have been used in past studies to successfully trace dust from source to sink (Goodman et al., 2019a). These fingerprints were identified through trace and major element chemistry and isotopes. Sequential leaching of dust samples is used to evaluate element availability or mobility in the environment, particularly for potentially harmful anthropogenic-enriched elements (Carling et al., 2012; Dastrup et al., 2018; Goodman et al., 2019). Variations in dust chemistry and largely characterized using trace element concentrations (Ben-Israel et al., 2015; Zhao et al., 2015). Principal component analysis (PCA) is often used to interpret large geochemical datasets and differentiate samples from various sources (Chen et al., 2022; Zeng et al., 2022).

Strontium isotope ($^{87}Sr/^{86}Sr$) ratios are a useful tool to track dust from source to sink. The $^{87}Sr/^{86}Sr$ ratios of dust depend on the geology of dust emission sources. $^{87}Sr/^{86}Sr$ ratios are a useful tool for tracking dust sources because they undergo minimal fractionation due to physical processes such as weathering (Flockhart et al., 2015). Strontium is geochemically like calcium, which allows the use of Sr as a proxy for Ca in many studies (Salifu et. al, 2018). Rubidium is geochemically like potassium and substitutes of K in K-bearing mineral lattices (Salifu et. al, 2018). ^{87}Rb undergoes radioactive decay to produce radiogenic ^{87}Sr, so K-bearing minerals like biotite, muscovite, and illite can result in higher $^{87}Sr/^{86}Sr$ ratios within the bulk rock composition (Salifu et. al, 2018). The $^{87}Sr/^{86}Sr$ ratios in these samples are a function of the complex mixture of minerals in dust, how old each one is, and their individual $^{87}Rb/^{86}Sr$ ratios ratios.$^{87}Sr/^{86}Sr$

ratios in carbonate minerals have been used to distinguish between playa dust sources and as tracers of dust-derived Sr in mountain watersheds (Carling et al., 2020; Dastrup et al., 2018). Sr isotopes measured in lake sediments and local volcanic bedrock in the San Juan Mountains in Colorado have been linked to exogenous sources, rather than locally eroded bedrock, implying long range dust transport to these areas (Neff et al., 2008). Tracing dust sources is also possible using radiogenic isotope compositions of the dust preserved in the paleoclimate record (Aarons et al., 2017).

Dust mineralogy is a useful tool for identifying dust sources. Variations in dust mineralogy on the regional scale can be subtle, but in some cases may be great enough to identify source areas (Lawrence and Neff, 2009). These concentrations vary due to different bedrock types and surficial geology. Heavy minerals are more resistant to mechanical breaking and chemical weathering, making them a good trace source of nearby sediments. Light minerals are a major component of eolian dust, which are likely sourced from sediments further away (Chen and Li, 2011). Published geologic maps are useful for determining surficial geology and underlying bedrock that control mineralogy.

Remote sensing and normalized difference vegetation index (NDVI) has been used to evaluate dust susceptibility in arid regions around the world (Kimura, 2012; Lee and Kim, 2012). NDVI using Landsat imagery is particularly useful for identifying areas with bare earth, indicating a greater potential for dust production (Xu et al., 2006). Understanding how vegetation cover changes seasonally can help determine how dust sources vary as these factors change. Maps of NDVI data are created using geographic information system (GIS) software to evaluate seasonal changes in vegetation (Borana and Yadav, 2018).

The purpose of our study is to develop a dataset of dust composition using samples from multiple land use types in dust-emitting regions across the western United States. Specific objectives are to: 1) develop isotopic, geochemical, and mineralogical fingerprints for characteristic dust sources; 2) investigate seasonality of fingerprints; and 3) create GIS maps of surrounding vegetation and surficial geology to better understand dust source regions. To accomplish these objectives, we measured trace and major element chemistry, $^{87}Sr/^{86}Sr$ ratios, and mineralogy in seasonal and interannual dust emission samples collected by the National Wind Erosion Research Network (NWERN). Additionally, we used remote sensing products and GIS software to characterize the geology and vegetation cover at each NWERN site. Better understanding of dust fingerprints from different source areas will inform dust tracking and future policy, helping make better decisions for hazard mitigation moving forward.

2. SITE DESCRIPTIONS

Dust samples for this study were provided by the National Wind Erosion Research Network (NWERN) and funded by the National Science Foundation (NSF). The NWERN was established in 2014 as a collaborative effort between departments to create a long-term research program to address critical challenges in wind erosion research and management in the United States (Webb et al., 2016). The network aims to provide data to help understand basic aeolian processes across various land use types and management practices, develop models to assess wind erosion and dust emissions, and encourage collaboration in the aeolian research community (Webb et al., 2016).

Site Descriptions

We obtained dust samples from ten NWERN sites across six states across the western United States (Figure 1). The samples were collected using modified Wilson and Cooke (MWAC) samplers (Webb et al., 2015) to capture dust and soil that are lofted and transported from their source area. The sites were chosen by NWERN with varying land use types and climate conditions for the purpose of our study (Table 1). We checked for seasonality for the sites that had multiple samples from multiple seasons. The sites that did not have sufficient data for multiple seasons were Akron, Lordsburg, and Mandan. We analyzed the geochemistry and microbial makeup of the dust provided to develop fingerprints to help us better understand dust sources and sinks in these areas. Each of the study sites are described below using information from the NWERN website (www.winderosionnetwork.org).

Colorado

Two of our sites were in the state of Colorado - Akron and the Central Plains Experimental Range (CPER). Each of these sites are located on the Central Great Plains Research station in a semi-arid climate, which consists of cold, dry winters and hot, dry summers. Both sites are managed by the USDA-ARS (United States Department of Agriculture - Agricultural Research service) LTAR (Long Term Agroecosystem Research) network.

Akron

The Akron site is a cropland agriculture site with no-till winters and a rotation of wheat, corn, and millet in the summer. This site is 7 km east of the town Akron, just 154 km southeast of the CPER site. The soils are loam to silty loam soils on the surface, which sit on tertiary aged loose to well-cemented sand and gravels. This site is surrounded by Tertiary aged ashy claystone, sandstones, and conglomerate units with abundant Quaternary eolian dune deposits consisting of

sand, silt, and Peoria loess (Figure 2) (USGS, 1979). Average annual precipitation is 421mm with most occurring between April and August. Temperature ranges from 15° C and 31° C in July and -9° C to 3.5° C in January. The terrain slope is 0% and nearby terrain slopes range between 0 and 3%.

Central Plains Experimental Range (CPER)

The Central Plains Experimental Range Network site is a rangeland research station grazed by cattle 40 km northeast of the town Greenly, Co. This site has similar soils to the Akron site, composed of a sandy clay loam above a fine sandy loam. With their similar climate, soil, and bedrock conditions, these sites provide a direct comparison between rangeland and cropland land use types in this area. This site is located on Quaternary aged alluviums and gravels surrounded by Tertiary aged ashy claystone, sandstones, and conglomerates and Upper Cretaceous shales, claystone, and sandstone in the Laramie Formation (Figure 3) (USGS, 1979). Average annual rainfall is 320mm with most occurring between April and September. Temperature ranges between 14° C and 34° C in July and -9° C to 8° C in January. The terrain slope is 0% with surrounding terrain slopes ranging from 0 to 15%.

Oklahoma

One site is in the state of Oklahoma- the Southern Plains site in El Reno.

Southern Plains - El Reno

The El Reno site is an agriculture site with a no-till wheat winter 50 km west of Oklahoma City. Like the Colorado sites, El Reno is managed by the USDA-ARS (LTAR)

network. The climate is temperate sub-humid, which lends itself to cool, dry winters, hot, wet summers and wet falls and springs. No research has been done regarding the soil type in this area, according to the NWERN site. But looking at the web soil survey through USDA, the soils for this area are classified as Norge silt loams with an average pH of 5.6. The El Reno site is on the eastern edge of the Anadarko Basin, bordering the Anadarko Shelf. The geology surrounding this site contains Permian aged bedrock composed of shales, sandstones, and gypsum, and Quaternary aged alluvium, dune sand, and volcanic ash. (Figure 4)(USGS, 1954). Average annual rainfall is 815mm with most occurring in the spring and summer. Temperature ranges from 0.5° C in January to 30° C in August. No slope has been recorded at this site.

New Mexico

Three of the sites we studied are in New Mexico state - Holloman Air Force Base (HAFB), Jornada Experimental Range (Jornada) and Lordsburg Playa (Lordsburg). Each of these sites is an arid to semi-arid climate.

Holloman Air Force Base (HAFB)

The Holloman Air Force Base site is located in the Tularosa Basin in the Chihuahuan Desert in south-central New Mexico. In addition to being a military airfield, the area is occasionally used as rangeland for cattle. The climate is arid to semi-arid with low annual precipitation and strongly biologically crusted cyanobacteria soils. Soils are gypsiferous fine to very fine sandy loams with a high gypsum content. This site is bounded on either side by the San Andres and Sacramento Mountains with White Sands National Monument directly to the west. The geology surrounding consists of Quaternary eolian, alluvium, and piedmont alluvial deposits

with Quaternary aged basaltic to andesitic lava flows in the north and Pennsylvanian aged limestone, sandstones, and shales in the Sacramento Mountains to the east (Figure 5) (USGS, 2003). Average annual rainfall is 278mm with most occurring between June and September. Temperature ranges between 25° C and 8.5° C year-round. The terrain slope is 0%

Jornada Experimental Range (Jornada)

The Jornada Experimental Range (LTAR) site is located in the Jornada Basin in south-central New Mexico in the northern Chihuahuan Desert. The basin is bounded by the Rio Grande Valley to the west and the San Andres Mountains to the east. This site is a rangeland research station grazed by cattle. The soils are mostly sandy loam to fine sandy loam with little to no biological crusting, but high calcium carbonate content. The surrounding geology consists of Quaternary sand, gravel, alluvium, and piedmont alluvial deposits. East and southeast of the site is composed of middle Pleistocene to upper Miocene aged sand and gravel from the Upper Santa Fe Group, with Tertiary aged intrusive igneous rocks, ranging from intermediate to silicic in composition. (Figure 6) (USGS, 2003). Average annual precipitation is 250mm with most occurring between June and September. Temperature ranges between 25° C and 5° C and the terrain slope is less than 0.5%.

Lordsburg Playa (Lordsburg)

The Lordsburg Playa Network site is located 20 km southwest of Lordsburg, New Mexico on a dry lakebed playa in the northern Chihuahuan Desert. Vegetation is very sparse, and the area is occasionally used for rangeland cattle grazing. The geology at the site is predominantly Quaternary lacustrine and playa deposits. The mountains surrounding the playa

are composed of Tertiary aged andesitic to dacitic lava flows, rhyolitic lavas and tuffs, and Quaternary piedmont alluvial deposits. South of the site consists of more basaltic to andesitic lava flows (Figure 7) (USGS, 2003). No information was provided on precipitation, temperature, or slope for this site.

North Dakota

One site is in North Dakota state - the Northern Plains site in Mandan.

Northern Plains - Mandan

The Mandan site is located on the Missouri Plateau in the Temperate Steppe Ecoregion of North Dakota 6 km south of Mandan. Mandan is part of the Long-Term Agroecosystem Research (LTAR) network and managed by the USDA Northern Great Plains Research Laboratory (NGPRL). This site has a semiarid continental climate where evaporation exceeds precipitation each year. This is an agriculture site that grows sunflowers, soybeans, wheat, and corn and consists of a silty loam soil at the surface. The geology at the site consists of predominantly Quaternary aged silts, clays, and glacial till. (Figure 8) (Murphy, 1999). Average temperature in the summer is 21° C and -11° C in the winter. The terrain slope is 0 to 3% characterized by rolling hills.

Utah

One site is in Utah state in Moab.

Moab

The Moab site is located on the Bartlett Flat in south-eastern Utah north of Canyonlands National Park and east of the Green River and Labyrinth Canyons. This site is a semi-arid climate with heavy rangeland use from cattle. The heavy grazing has resulted in a lack of biological crust on the soils, which is characteristic for other areas in Moab. The geology here reflects that of the Colorado Plateau, including Quaternary eolian deposits and characteristic units such as the Navajo sandstone, Entrada sandstone, Morrison Formation, and Kayenta Formations (Figure 9) (Doelling, 2002). Temperature ranges between 19° C and 33° C in July and -6° C to 3° C in January. The terrain slope is less than 1%.

Nevada

Two of our sites are in Nevada state - Red Hills and Twin Valley. Each of these sites are rangeland areas grazed by cattle and wild horses and are located relatively close to each other. Both sites are run by the USDA-ARS Great Basin Rangelands Research unit in Reno, Nevada, and the Bureau of Land Management (BLM) office in Winnemucca, Nevada. Average annual precipitation is 200mm, most of which occurs as winter snow. Temperatures range from 7° C to 10° C year-round. The climate is semi-arid with warm, dry summers. Both sites were affected by the Martin Fire in July of 2018, which burned almost 100% of the area surrounding Red Hills and Twin Valley.

Red Hills

The Red Hills site is in north central Nevada on the foot slope of a fan remnant within a complex mix of low hills and alluvial fans, 30 km northeast of Paradise Valley, Nevada. Surface soils here consist of loams that previously had biological crusts before the fire. The surrounding

geology consists of middle to late Miocene basalt and rhyolitic flows, beach and dune sand deposits, and welded to non-welded silicic ash flow tuffs (Figure 10) (Stewart and Carlson, 1978).

Twin Valley

The Twin Valley site is in north central Nevada on a plateau about 28 km south of the border between Nevada, Oregon, and Idaho. Twin Valley has similar climate and soil composition to the Red Hills site, due to their proximity. This site is located on the Brandbury formation, which consists of middle to late Miocene basalts, gravels, tuffaceous sediments and scattered beach and dune sand deposits (Figure 11) (Stewart and Carlson, 1978).

3. MATERIALS AND METHODS

3.1 Sample Collection

To evaluation dust emissions across the western US, samples were obtained from ten representative NWERN sites. The NWERN samples collected for analysis ranged across three years (2018-2020) and were consolidated by season (Spring, Summer, and Fall). Spring samples were collected from March – May, Summer samples were collected from June – August, and Fall samples were collected from September – November. NWERN samples were collected using Modified Wilson and Cook samplers (MWAC). Each site consisted of three MWAC samplers randomly placed in a grid cell of a one hectare 3 x 3 grid, with a mast and wind vane installed to direct the airborne sediment into the collectors. These samplers contain collectors situated at four different heights (10cm, 25cm, 50cm, 80cm) to measure horizontal dust flux (Webb et al., 2015), which were collected monthly. Dust was processed from the highest two

MWAC containers because dust particles higher from the soil surface are more representative of dust suspended over longer distances, due to their smaller grain sizes. These collectors were emptied according to NWERN protocols and stored in clean plastic vials and bags before being shipped to Brigham Young University for analyses. These samples were analyzed as a total bulk sample.

3.2 Laboratory analyses

To measure the trace and major element concentrations in the NWERN samples, an acid dilution was performed to prepare samples for inductively coupled plasma mass spectrometry (ICP-MS). Dust samples were analyzed following a one-step aqua regia leaching procedure. The total concentration of each element was calculated from the sum of this step. 50 mg of dust from each sample was separated into 15 mL centrifuged tubes, which had been previously sterilized with 10% HCl, heated for 48 hours at 60°C (rotated every 24 hours), and rinsed with Milli-Q water and dried. Aqua regia was added to each sample (1.33 mL HCl and 0.67 mL HNO3 -2 mL of aqua regia total), and the sample was stirred vigorously. Samples were left to equilibrate for ~24 hours, followed by centrifugation at 3000 rpm for 5 minutes. After centrifugation 1.6 mL of this centrifuged aqua regia was pipetted off into a new tube. The original sample was rinsed with Milli-Q water filled to the 5 mL line in each tube and centrifuged again with the same parameters. The process was repeated twice, pipetting off 4.5 mL of the centrifuged liquid from each sample into the new tubes. This resulted in ~10.5 mL of each acid digested dust sample, which were stored in the fridge until they were transported to the University of Utah for ICP-MS analysis. At the University of Utah, 1 mL of the sample was pipetted off into a new tube and mixed with 100 mL of indium, which is used as an internal standard during the process. These

new tubes were filled to the 10 mL line with 2.4% HNO3 TMG and the resulting liquid was transferred into grid trays to be loaded into the ICP-MS.

The leachate was analyzed for trace and major element concentrations using an Agilent 8900 triple quadrupole ICP-MS at the ICP-MS labs, Department of Geology and Geophysics, University of Utah (https://earth.utah.edu/research_facilities/earth-core-facility/icp-ms.php). Concentrations were quantified using and external calibration curve for the following 44 elements: Li, Be, B, Na, Mg, Al, K, Ca, Sc, V, Cr, Mn, Fe, Co, Ni, Cu, Zn, Se, Rb, Sr, Y, As, Mo, Cd, Sb, Cs, Ba, La, Ce, Pr, Nd, Sm, Eu, Gd, Tb, Dy, Ho, Er, Yb, Lu, Tl, Pb, Th, and U. The external calibration curve was prepared from 1,000 mg/L single-element standards (Inorganic Ventures, Christiansburg, VA, USA), with maximum concentrations around 0.1 mg/mL for trace and 10 mg/mL for major elements. Masses 7, 9, 11, and 27 under no-gas mode were used for Li, Be, B and Al respectively. Masses 39, 56 and 78 under H_2 mode were used for K, Fe and Se respectively. Masses 23, 24, 45, 51, 52, 55, 59, 60, 63, 66, 85, 88, 89, 95, 111, 121, 133, 137, 139, 140, 141, 146, 147, 153, 157, 159, 163, 165, 166, 172, 175, 205, 208, 232 and 238 under He mode were used for Na, Mg, Sc, V, Cr, Mn, Co, Ni, Cu, Zn, Rb, Sr, Y, Mo, Cd, Sb, Cs, Ba, La, Ce, Pr, Nd, Sm, Eu, Gd, Tb, Dy, Ho, Er, Yb, Lu, Tl, Pb, Th, and U respectively. Masses 44>44 and 75>91 under O_2 mode were used for Ca and As. Diluted samples, calibration solutions, reference solution and blanks, were added 10 ng/mL In as internal standard and run in the ICP-MS using a dual pass quartz spray chamber: PTFE nebulizer and dual-syringe introduction system (Teledyne, AVX 71000), platinum cones and sapphire injector in a platinum-shielded quartz torch. Limit of determinations for each element were calculated as three times the standard deviation of the background, multiplied by the total dilution factor used for samples (~2,000). A standard reference solution (SRM 1643f, Trace Elements in Water, National Institute

of Standards and Technology, Gaithersburg, MD) was analyzed multiple times in each run together with the samples as a continuing calibration verification. The long-term reproducibility for SRM 1643f shows that our results are accurate within 5% for most elements. The ICP-MS instrument is in a filtered air positive pressure lab and sample handling and dilutions were performed in laminar flow benches and using calibrated pipettors (Eppendorf Reference, Hamburg, Germany).

To characterize mineralogy in the NWERN dust samples, X-ray Diffraction (XRD) was used. This was evaluated as bulk sample as not enough samples were provided to separate out bulk from fine material (85 samples in total). Sample preparation involved grinding down dust samples with methanol, evaporating off the alcohol, then grinding down again with hexane and evaporating off the remaining alcohol. Dust samples were then pushed through a 250-micron sieve and stored in clean bottles for later XRD analysis. Samples were analyzed on zero background holders with a Rigaku MiniFlex 600 XRD. Resulting patterns were quantitatively interpreted from the Reference Intensity Ratio (RIR) method with the Rigaku PDXL2 software. For the RIR method, weight ratios are calculated from given intensity ratios of the substance normalized to a known standard and its highest peak intensity (Hubbard et al., 1976).

To understand how isotopic fingerprints are unique to each area, strontium isotope ($^{87}Sr/^{86}Sr$) ratios were analyzed using the same leachate used for the trace and major element analysis. One or two dust samples from each site (n = 13) were analyzed for $^{87}Sr/^{86}Sr$ ratios on the aqua regia leachate using a MC-ICP-MS. These samples were processed the same way as outlined in (Carling et al., 2020). The samples were purified inline using a Sr-FAST ion chromatographic column packed with a crown ether resin (Mackey and Fernandez, 2011). Results were interpreted by plotting each of the $^{87}Sr/^{86}Sr$ ratios against each other and comparing

bedrock ages at each site and the surrounding area (Figure 16). During the analyses reported herein, we determined the $^{87}Sr/^{86}Sr$ ratio of the standard reference material SRM987 (certified value of 0.71034 ± 0.00026) to be 0.710300 ± 0.000008 (n = 13; mean ± standard deviation). The $^{87}Sr/^{86}Sr$ ratios were corrected for mass bias using an exponential law, normalizing to $^{86}Sr/^{88}Sr = 0.1194$ (Steiger and Jäger, 1977). Isobaric interferences on the $^{87}Sr/^{86}Sr$ ratios, such as from ^{87}Rb and ^{86}Kr, were corrected by simultaneously monitoring ^{85}Rb and ^{83}Kr using the corresponding invariant ratios of $^{87}Rb/^{85}Rb = 0.385706$ and $^{86}Kr/^{83}Kr = 1.502522$ (Steiger and Jäger, 1977).

3.3 Normalized Difference Vegetation Index (NDVI) maps of sample sites

To understand how vegetation cover changes over time, Landsat 8 imagery was used to create raster layers displaying vegetation for each season at every sample site (Figure A1). This was done using imagery found on Earth Explorer. Images for each season were chosen based on the following criteria: less than 10% cloud cover, appropriate season (Spring = March - May, Summer = June - August, Fall = September - November), had Bands 4 (RED) and Band 5 (NIR) for NDVI analysis. Images chosen were consistent with the years and seasons the dust was sampled. In some instances (Moab), two Landsat images from different days were mosaicked together to cover the entire area of interest. Each of these images were uploaded into ArcGIS Pro where a Model Builder code was used to calculate the Normalized Difference Vegetation Index (NDVI) (Figures 12 and 14). This was calculated using Eqn 1 below by inputting the RED and NIR bands for each raster and setting parameters as found in (Heidarian et al., 2018).

$$NDVI = \frac{(\mathrm{NIR} - \mathrm{RED})}{(NIR + RED)}$$

The resulting rasters were colored for easier interpretation and compared over time.

3. 4 Geologic maps of study sites

Geologic maps for each study site were compiled and manipulated using ArcGIS Pro and Adobe Illustrator (Figures 2-11). Reference maps were found on state geologic survey websites or provided by the United States Geological Survey (USGS). Often GIS databases and shapefiles were unavailable, and pdfs of geologic maps were georeferenced and traced to create unique polygon feature classes. Unit descriptions for these maps were taken from the original map pdfs. Colors were standardized according to the official USGS colors for easier comparison across all maps.

3.5 Principal component analysis (PCA)

A principal component analysis (PCA) was run on the trace and major element chemistry using MATLAB. The data was cleaned up by removing all the nan values and replacing them with the minimum value of the element divided in half. The data was z-scored and run through a PCA. Using the table of trace and major element results, this displayed and compared all the samples against each other and helped with the interpretation of trends in elemental composition between the different sites (Figure 13). For this study, sample DTL-14 was excluded from the PCA because of its unusually high concentrations of Cu. This was likely due to contamination, as none of the other samples at this site contain large concentrations of Cu.

4. RESULTS

4.1 Strontium isotope (87Sr/86Sr) ratios show spatial variability in dust sources

Strontium isotope ($^{87}Sr/^{86}Sr$) ratios showed distinct differences in dust sources based on the local bedrock and sediment sources. Dust samples from the oldest bedrock generally had the

highest $^{87}Sr/^{86}Sr$ ratios, and samples from the youngest bedrock had the lowest ratios (Figure 16). These can be explained by their mineral composition and overall age of the samples. Some exceptions included El Reno, Moab, and Lordsburg where the dust consisted of sediments derived from a mixture of older and younger bedrock or contained minerals with K and Ca, causing the $^{87}Sr/^{86}Sr$ ratios to be higher for samples containing more K-bearing minerals, and lower for samples containing more Ca-bearing minerals.

Strontium isotope ($^{87}Sr/^{86}Sr$) ratios varied across NWERN sample sites according to local bedrock ages and the influence of surficial sediments. Bedrock ages ranged from Permian to Holocene and generally plotted oldest to youngest, with a few exceptions. The Colorado sites (CPER and Akron) are both located in NE Colorado with the CPER site located on Late Cretaceous shale bedrock (Figure 3)(USGS, 1979), while the Akron site sits on younger, Pliocene Sandstone (Figure 2)(USGS, 1979). The CPER $^{87}Sr/^{86}Sr$ ratio (~0.714) was higher than the $^{87}Sr/^{86}Sr$ ratio for Akron (~0.713) because of its older bedrock source.

The strontium isotope (87Sr/86Sr) ratio at Lordsburg, NM was higher than expected (~0.712) given that the site is located on a playa that consists of Holocene lake deposits. Holocene sediments should have a lower $^{87}Sr/^{86}Sr$ ratio if they are sourced from young rocks. However, the bedrock surrounding the playa contains Oligocene and Cretaceous aged igneous rocks (Figure 7) (USGS, 2003) that may contribute to relatively high $^{87}Sr/^{86}Sr$ ratios. The Lordsburg playa sample was 16% muscovite, a K-bearing mineral that may also contribute to a higher $^{87}Sr/^{86}Sr$ ratios.

El Reno, OK consists of two different samples - one taken in the spring, and one taken in the fall. These plots are in two very different places in Figure 16. The bedrock under El Reno is Permian aged shales, the oldest bedrock from all the sites sampled (Figure 4). However, the $^{87}Sr/^{86}Sr$ ratio here is lower than expected (~0.711 - 0.709). The El Reno site is surrounded by

Holocene alluvium, which is likely mixing with older bedrock and bringing the $^{87}Sr/^{86}Sr$ value down. In the spring, this $^{87}Sr/^{86}Sr$ value is substantially lower, which is likely from more mixing and higher concentrations of carbonate minerals in the soil due to seasonal carbonate precipitation when the soil is dryer. These carbonate minerals in the spring samples are composed of more Ca-bearing minerals, such as gypsum, calcite, and dolomite, which may also contribute to a lower $^{87}Sr/^{86}Sr$ ratio.

The Moab, UT site is on Holocene eolian sand deposits and is surrounded by Lower Jurassic aged Navajo Sandstone (Doelling, 2002). Mixing from this older bedrock unit is a likely cause for a higher $^{87}Sr/^{86}Sr$ ratio value with relation to the other sample sites. These samples also contain muscovite and illite, K-bearing minerals that could contribute to a higher $^{87}Sr/^{86}Sr$ ratio with relation to the other NWERN sites.

The Jornada, NM site consists of Holocene alluvial deposits, with both the spring and fall sample compositions remaining relatively consistent (USGS, 2003). Seasonal changes may cause mixing from the Middle Pleistocene sandstones in the nearby Upper Santa Fe Group that could account for the slight difference between spring and fall samples

The Twin Valley, NV, and Red Hills, NV sites are relatively close to each other, but differ in their bedrock type. The Twin Valley site is located on Miocene aged basalts while the Red Hills site is located on Pliocene coarse to fine detrital (Stewart and Carlson, 1978). The Twin Valley bedrock is slightly older, which likely explains its higher $^{87}Sr/^{86}Sr$ ratio relative to Red Hills. Twin Valley also contained microcline and muscovite, K-bearing minerals that could contribute to a higher $^{87}Sr/^{86}Sr$ ratio here than in Red Hills

4.2 Trace and major element chemistry shows variability across NWERN sites

Dust from each of the NWERN sites has distinct trace and major element chemistry with some overlap between the different sites. The Mandan, ND site had distinct chemistry relative to other sites with high concentrations of metals Cr, Fe, Co, and Ni, suggesting anthropogenic inputs or elevated, naturally occurring metals in the soil (Jyoti et al., 2015). Lordsburg playa also had distinct chemistry relative to other sites with higher concentrations of all 40+ trace and major element concentrations analyzed, with especially high concentrations of Li, Na, Mg, Ca, and Sr, which are more common playa elements. Seasonal variation for various elements at HAFB and El Reno sites was also found. HAFB had seasonal spikes in Li, Na, Mg, Ca, and Sr during the spring and summer months, which could be attributed to seasonal, gypsum-rich inputs from the adjacent White Sands National Park. El Reno had seasonal spikes in Na, Mg, Al, K, Ca, Cu, Zn, and Sr during the spring months, which drop again in the fall. This could be due to changing agricultural processes throughout the year, or carbonate dissolution and precipitation cycles with the wet and dry seasons.

4.3 Principal component analysis (PCA) shows distinction between playa influenced sites compared to others

The PCA showed distinction between playa-influenced sites and all others. In the PCA, HAFB and Lordsburg plotted separately from the other sites (Figure 13a). PC1 explains 58.07% of the variation, being most influenced by Be, Al, K, Sc, (Fe), Rb, As, Cs, and REE+Y. PC2 explains 13.83% of the variation and is most influenced by Li, Na, (Mg), Ca, Cr, Cu, Se, Sr, and Mo. In the trace and major elements, the PCA showed a distinct separation for HAFB and Lordsburg from the other eight sites along PC2. Dust from Lordsburg contains the highest concentrations of playa elements Li, Na, Mg, and Sr. The HAFB dust shows enrichment in Na,

Mg, and Sr during the spring due to SW winds adding gypsum and other playa elements from White Sands National Park. Dust enriched in these playa elements, as shown through the PCA, shows a distinct fingerprint when compared to the agricultural and rangeland land use types. These clusters along PC2 are likely correlated with regional weathering intensity, as derived from the amount of quartz and feldspars in the dust mineralogy (Figure 14).

The other eight agriculture and rangeland land use types were run through the PCA again without the HAFB and Lordsburg samples (Figures 13b and 13c). In Figures 13b and 13c, PC1 explains 61.13% of the variation, being most influenced by Li, Be, K, Sc, V, Mn, Fe, Co, Rb, As, and REE+Y. PC2 explains 8.38% of the variation and is most influenced by Cr, Ni, Se, Mo, Cd, Tl, and Pb. PC3 explains 6.93% of the variation and is most influenced by Na, Mg, Al, Ca, Cu, Sr, and -Sb. The Mandan samples plot high on PC2 due to their enrichment in Cr, Ni, Tl, and Pb relative to the other sites (Figure 13b). In Jornada, the spring samples plot higher on PC1 due to being more enriched in Li, Be, K, V, Mn, and Fe than the fall and summer samples there (Figure 13b). The spread across PC2 in the Akron samples can be explained by the higher concentrations of Cr, Ni, Tl, and Pb present in the spring 2019 samples than the spring 2020 samples (Figure 13b). In Figure 13c, fall samples from Moab, Jornada, and El Reno plot higher on PC3 due to being more enriched in Na, Al, Mg, Ca, and Sr (Tables A1 and A4).

4.4 Mineralogy shows seasonal variation in individual sites and common minerals found at all sites.

Mineralogy showed similarities across all sites with distinct variation within individual sites. All sites contained quartz, phyllosilicates, and feldspar minerals. Other sites showed distinct minerals that varied with the underlying bedrock, with some sites showing seasonal

variability. El Reno shows carbonates in the spring that do not show up in the fall sample. HAFB shows an increase of gypsum in the spring that decreases drastically in the fall. El Reno, HAFB, Jornada, Lordsburg, and Moab all contain calcite with HAFB also containing calcium sulfate and iron oxide minerals (Figure 15). Averaged mineralogy results for each NWERN study site can be found Figure 14.

5. DISCUSSION

5.1 Factors influencing fingerprints across dust sources

Geochemical, mineralogical, and isotopic data are useful to fingerprinting sites based on their geology. However, these measurements are not always useful for distinguishing between distinct land use types. For example, the Akron and CPER sites have similar $^{87}Sr/^{86}Sr$ ratios, geochemistry, and mineralogy, but different land use types. The Akron and CPER sites in Colorado also exhibit very similar climate, soils, and bedrock conditions. Akron is an agricultural site, while CPER is a rangeland site. Because of the proximity to one another, the bedrock geology remains constant, with dust from each site containing similar amounts of muscovite, calcic plagioclase, sodic plagioclase, and quartz (Figure 15). The trace and major element composition on the PCA (Figure 13a) shows each site is similarly enriched in PC2 playa elements. There is some distribution across PC1 (Figure 13b), which is due to more enrichment of PC1 elements (Fe, Mn, REE+Y, etc.) in Akron than CPER, which is why Akron plots higher on this axis. These two sites are geochemically similar. Their resulting $^{87}Sr/^{86}Sr$ ratios reflect a consistent dust source for each of the two sites (CPER ~0.714, Akron ~0.713). Due to the abundant similarities between these two sites, another method is needed to create a unique fingerprint. Microbial fingerprints for these same samples show distinct microbiomes in the

Akron samples associated with the presence of heavy metals or anaerobically digested slurry. This is attributed to mixtures in fertilizers due to agriculture (*In prep:* Leifi, 2023). These same microbiomes are not found in the CPER site, allowing a distinction between agricultural and rangeland sites. Microbial analyses such as this one is invaluable in creating unique dust fingerprints for different land use sites like these that are so geochemically similar.

Another example where the geochemistry alone was not sufficient to differentiate between sites was with the Nevada NWERN samples. In the Black Rock volcanic field in Nevada, especially low $^{87}Sr/^{86}Sr$ ratios have been observed (~0.703) due to younger bedrock ages (<600 ka) (Rasoazanamparany et al., 2015). The Red Hills and Twin Valley sites are rangelands that lie on Miocene-aged basalts and dune deposits, so low $^{87}Sr/^{86}Sr$ ratios are expected in these volcanic rocks (Red Hills ~0.7075, Twin Valley ~0.7076). The $^{87}Sr/^{86}Sr$ ratios measured in each sample were the similar, likely due to the similarly aged bedrock in the surrounding area (Figures 10 & 11). Both sites were affected by a regional wildfire that burned all the surrounding area. With these similarities, it is likely their mineralogical and geochemical fingerprints would be the same. However, this was not the case. Each site has the same abundance of quartz with are varying amounts of sodic and calcic plagioclases (Figure 15). Twin Valley also includes muscovite, microcline, and calcic plagioclase, while Red Hills includes palygorskite and more sodic plagioclase. These differences can be attributed to their location on the bedrock. The Twin Valley site is located on basalt, gravel, and tuffaceous sediments, which likely includes more calcic rich plagioclase from mafic igneous rocks (Figure 11). The Red Hills site is located on the alluvial beach and sand dune deposits, which likely include more clay-rich palygorskite minerals and sodic plagioclase (Figure 10). In the PCA graph (Figure 13b), each site

is similarly enriched in PC2 playa elements with variation along PC1 due to differences in Na and Ca concentrations from local surficial sediments, as seen in the mineralogy discussed above.

5.2 Seasonality of fingerprints

Most of the NWERN sites showed consistent fingerprints throughout the year, but a few sites had seasonal variation in specific measurements. Both the El Reno, OK and HAFB, NM sites exhibited seasonal variability either in their mineralogy or their $^{87}Sr/^{86}Sr$ values, which indicates seasonal changes in dust sources for these regions.

HAFB had consistent $^{87}Sr/^{86}Sr$ values between fall and spring samples, but differing mineralogy. In Figure 14 we see an increase in gypsum in the spring that drastically drops in the fall. Seasonal changes in wind direction show a SW prevailing wind in the spring and an SSE prevailing wind in the fall (https://weatherspark.com/y/145618/Average-Weather-at-Holloman-Air-Force-Base-New-Mexico-United-States-Year-Round). The gypsum-rich White Sands National Park is located west of the HAFB sample site, which is likely the primary source of gypsum for our spring sample. Changing wind directions in the fall means less gypsum-rich dust from the gypsum dunes are introduced into the sample.

El Reno exhibited changes both in mineralogy and $^{87}Sr/^{86}Sr$ values in the fall and spring samples. Carbonate minerals such as dolomite, calcite, and gypsum are present in the spring sample that are not present in the fall sample (Figure 14). Oklahoma experiences wet summers and dry winters (Figure A1). Changes in carbonate precipitation and dissolution in the soils with these wet and dry seasons could explain this discrepancy. Carbonate dissolution in the soils happens during the summer months when soil moisture is at its peak with agriculture activity. Carbonate precipitation occurs when soil is actively drying in the winter to spring months, which

likely increases carbonate minerals in our spring sample. This cycle of carbonate precipitation and dissolution in the soil is further supported by a low soil pH (pH = 5.6) as recorded by the USDA.

5.3 Comparison of methods and results to similar studies

Previous studies conducted by Aarons et al., 2017 and Munroe et al., 2020 successfully used isotopic, geochemical, and mineralogical fingerprints to trace dust. In Aarons, 2017, dust source regions heavily affected by known dust events, increased human settlement, and livestock grazing. Sampling the top 5 cm of topsoil and separating sediment into size fractions, Aarons was able to perform analyses with the size fraction most representative of airborne dust. Aarons found distinct $^{87}Sr/^{86}Sr$ ratios for each of the five regions studied. In the Colorado Plateau, $^{87}Sr/^{86}Sr$ ratios ranged from 0.707987 to 0.717230, which aligns with the $^{87}Sr/^{86}Sr$ value for our Moab NWERN site ($^{87}Sr/^{86}Sr = 0.70938$). In the San Luis Valley, $^{87}Sr/^{86}Sr$ ratios ranged from 0.712177 to 0.740236, which fits with the $^{87}Sr/^{86}Sr$ value for Lordsburg playa on the lower end of that range in that region ($^{87}Sr/^{86}Sr = 0.71225$). These consistencies validate our sampling and lab methods and further confirm the influence of surficial sediments, or eroded bedrock, on $^{87}Sr/^{86}Sr$ ratios. The study concluded that future work and research is still needed in the understanding isotopic compositions of transportable dust from known dust source areas (Aarons et al., 2017).

In Munroe, 2020, the focus was on dust deposition in the Uinta Mountains. Sampling surficial sediments in both the Uinta Mountains and arid regions in the western United States, Munroe found significant exotic dust deposition in the mountains from these arid regions. The results showed the trace and major element chemistry, as well as Sr and Nd isotope

compositions, of the A soil horizon most closely resembled dust, while the B soil horizons more closely resembled bedrock (Munroe et al., 2020). Using a PCA, Munroe found that PC-1 was influenced by Na, Sr, Mg, and Ca, more typical dust elements, while PC-2 was influenced by Fe, Ti, K, Zr, Rb, and Al, more typical bedrock elements. Our PCA also clumped Li, Na, Mg, and Ca into one principal component with Fe into the other. This has implications for our study, interpreting that NWERN sites that plot higher on the principal component controlled by dust elements are more like dust, while NWERN sites that plot higher on the principal component controlled by bedrock are more compositionally like local bedrock. HAFB and Lordsburg playa plot the highest on the dust-controlled principal component axis and are therefore more likely influenced by eolian dust. The rest of the NWERN sites plot much lower on this axis, which could tell us that their compositions are more influenced by local bedrock. Lordsburg may be the exception to this, with it plotting high on both PC-1 and PC-2, implying more equal inputs from bedrock and eolian dust sources.

6. CONCLUSION

Our dataset has implications for characterizing dust sources across the western US and identifying characteristics that may be used for source tracking dust events. Dust events have many negative effects on human health and the environment, so it is vital that more information about dust composition and factors that control dust sources is obtained. $^{87}Sr/^{86}Sr$ ratios, geochemistry, and mineralogy are useful tools to understand dust composition. Changes in dust composition can be correlated with changing wind patterns, local or regional bedrock geology, and seasonal vegetation changes. Comparing our results to similar, successful studies on dust in

this region of the world will help refine our methods and create a dataset of potential dust source regions to be utilized in future work.

7. LITERATURE CITED

Aarons, S. M., Blakowski, M. A., Aciego, S. M., Stevenson, E. I., Sims, K. W. W., Scott, S. R., and Aarons, C., 2017, Geochemical characterization of critical dust source regions in the American West: Geochimica et Cosmochimica Acta, v. 215, p. 141-161.

Abed, R. M. M., Ramette, A., Hübner, V., De Deckker, P., and de Beer, D., 2012, Microbial diversity of eolian dust sources from saline lake sediments and biological soil crusts in arid Southern Australia: FEMS Microbiology Ecology, v. 80, no. 2, p. 294-304.

Ben-Israel, M., Enzel, Y., Amit, R., and Erel, Y., 2015, Provenance of the various grain-size fractions in the Negev loess and potential changes in major dust sources to the Eastern Mediterranean: Quat. Res., v. 88, p. 105-115.

Borana, S.L., and Yadav, S.K., 2018, NDVI-based vegetation changes and seasonal variation in semi-arid region, Remote Sensing Group, Defence Laboratory, Jodhpur-342011

Brahney, J., Mahowald, N., Ward, D. S., Ballantyne, A. P., and Neff, J. C., 2015, Is atmospheric phosphorus pollution altering global alpine Lake stoichiometry?: Global Biochem Cycles, v. 29, p. 1369–1383.

Carling, G. T., Fernandez, D. P., and Johnson, W. P., 2012, Dust-mediated loading of trace and major elements to Wasatch Mountain snowpack: Sci. Total Environ, v. 432, p. 65–77.

Carling, G. T., Fernandez, D. P., Rey, K. A., Hale, C. A., Goodman, M. M., and Nelson, S. T., 2020, Using strontium isotopes to trace dust from a drying Great Salt Lake to adjacent urban areas and mountain snowpack: Environmental Research Letters, v. 15, no. 11.

Chen, H., Wu, D., Wang, Q., Fang, L., Wang, Y., Zhan, C., Zhang, J., Zhang, S., Cao, J., Qi, S., and Liu, S., 2022, The Predominant Sources of Heavy Metals in Different Types of Fugitive Dust Determined by Principal Component Analysis (PCA) and Positive Matrix Factorization (PMF) Modeling in Southeast Hubei: A Typical Mining and Metallurgy Area in Central China, International Journal of Environmental Research and Public Health, Volume 19.

Chen, J., and Li, G., 2011, Geochemical studies on the source regio of Asian dust: Science China Earth Sciences, v. 54, p. 1279-1301.

Dastrup, D. B., 2016, Variations in Geochemistry and Mineralogy of Aeolian Dust Deposition to Mountains in Utah and Nevada, USA [Master of Science: Brigham Young University, 46 p.

Dastrup, D. B., Carling, G. T., Collins, S. A., Nelson, S. T., Fernandez, D. P., Tingey, D. G., Hahnenberger, M., and Aanderud, Z. T., 2018, Aeolian dust chemistry and bacterial communities in snow are unique to airshed locations across northern Utah, USA: Atmospheric Environment, v. 193, p. 251-261.

Derbyshire, E., 2007, Natural minerogenic dust and human health: Ambio, v. 36, p. 73-77.

Doelling, H. H., 2002, Geologic map of the Moab and Eastern part of the San Rafael desert 30’X 60’ quadrangles, Grand and Emery counties, Utah, and Mesa county, Colorado: Utah Geological Survey.

Flockhart, D. T. T., Kyser, T. K., Chipley, D., Miller, N. G., and Norris, D. R., 2015, Experimental evidence shows no fractionation of strontium isotopes (87Sr/86Sr) among soil, plants, and herbivores: implications for tracking wildlife and forensic science: Isotopes in Environmental and Health Studies, v. 51, no. 3, p. 372-381.

Goodman, M., Carling, G., Fernandez, D., Rey, K., Hale, C., Bickmore, B., Nelson, S., and Munroe, J., 2019a, Trace element chemistry of atmospheric deposition along the Wasatch Front (Utah, USA) reflects regional playa dust and local urban aerosols: Chemical Geology, v. 530, p. 119317.

Goodman, M. M., Carling, G. T., Fernandez, D. P., Rey, K. A., Hale, C. A., Bickmore, B. R., Nelson, S. T., and Munroe, J. S., 2019b, Trace element chemistry of atmospheric deposition along the Wasatch Front (Utah, USA) reflects regional playa dust and local urban aerosols: Chemical Geology, v. 530.

Guinoiseau, D., Singh, S. P., Galer, S. J. G., Abouchami, W., Bhattacharyya, R., Kandler, K., Bristow, C., and Andreae, M. O., 2022, Characterization of Saharan and Sahelian dust sources based on geochemical and radiogenic isotope signatures: Quaternary Science Reviews, v. 293, p. 107729.

Heidarian, P., Azhdari, A., Joudaki, M., Khatooni, J. D., and Firoozjaei, S. F., 2018, Integrating Remote Sensing, GIS, and sedimentology techniques for identifying dust storm sources: A case study in Khuzestan, Iran - Journal of the Indian Society of Remote Sensing: SpringerLink.

Hubbard, C. R., Evans, E. H., and Smith, D. K., 1976, The reference intensity ratio, I/Ic, for computer simulated powder patterns: Journal of Applied Crystallography, v. 9, p. 169-174.

Jyoti, V., Saini-Eidukat, B., Hopkins, D., and DeSutter, T., 2015, Naturally elevated metal contents of soils in northeastern North Dakota, USA, with a focus on cadmium: J Soils Sediments, v. 15, no. 7, p. 1571-1583.

Kellogg, C. A., and Griffin, D. W., 2006, Aerobiology and the global transport of desert dust: Trends Ecol. E, v. 21, p. 638-644.

Kimura, R., 2012, Effect of the Strong Wind and Land Cover in Dust Source Regions on the Asian Dust Event over Japan from 2000 to 2011: SOLA, v. 8, p. 77-80.

Kumar, R. S., and Rajkumar, P., 2014, Characterization of minerals in arid dust particles in the state of Tamilnadu, India through FTIR, XRD, and SEM analyses: Infrared Physics & Technology, v. 67, p. 30-41.

Lawrence, C. R., and Neff, J. C., 2009, The contemporary physical and chemical flux of aeolian dust: a synthesis of direct measurements of dust deposition: Chem. Geol, v. 267, p. 46-63.

Lee, J.-J., and Kim, C.-H., 2012, Roles of surface wind, NDVI and snow cover in the recent changes in Asian dust storm occurrence frequency: Atmospheric Environment, v. 59, p. 366-375.

Mackey, G. N., and Fernandez, D., High throughput Sr isotope analysis using an automated column chemistry system2011.

McTainsh, G., and Strong, C., 2007). The role of Aeolian dust in ecosyste: Geomorphology, v. 89, p. 39-54.

Menéndez, I., Pérez-Chacón, E., Mangas, J., Tauler, E., Engelbrecht, J. P., Derbyshire, E., Cana, L., and Alonso, I., 2014, Dust deposits on La Graciosa Island (Canary Islands, Spain): Texture, mineralogy and a case study of recent dust plume transport: CATENA, v. 117, p. 133-144.

Middleton, N. J., and Goudie, A. S., 2001, Saharan dust: sources and trajectories: Transactions of the Institute of British Geographers, v. 26, p. 165-181.

Munroe, J. S., Norris, E. D., Olson, P. M., Ryan, P. C., Tappa, M. J., and Beard, B. L., 2020, Quantifying the contribution of dust to alpine soils in the periglacial zone of the Uinta Mountains, Utah, USA: Geoderma, v. 378, p. 114631.

Murphy, E. C., 1999, Surface Geology Mandan Quadrangle, North Dakota: North Dakota Geological Survey.

Nakano, T., Yokoo, Y., Nishikawa, M., and Koyanagi, H., 2004, Regional Sr–Nd isotopic ratios of soil minerals in northern China as Asian dust fingerprints: Atmospheric Environment, v. 38, no. 19, p. 3061-3067.

Neff, J. C., Ballantyne, A. P., Farmer, G. L., Mahowald, N. M., Conroy, J. L., Landry, C. C., Overpeck, J. T., Painter, T. H., Lawrence, C. R., and Reynolds, R. L., 2008, Increasing eolian dust deposition in the western United States linked to human activity.

Négrel, P., and Petelet-Giraud, E., 2005, Strontium isotopes as tracers of groundwater-induced floods: the Somme case study (France): Journal of Hydrology, v. 305, no. 1, p. 99-119.

Painter, T. H., Barrett, A., Landry, C. C., Neff, J. C., Cassidy, M., Lawrence, C. R., McBride, K., and Farmer, G. L., 2007, Impact of disturbed desert soils on duration of mountain snow cover: Geophys. Res. Lett., v. 34.

Painter, T. H., Deems, J. S., Belnap, J., Hamlet, A. F., Landry, C. C., and Udall, B., 2010, Response of Colorado River runoff to dust radiative forcing in snow: PNAS, v. 107.

Pope, C. A., Dockery, D. W., Spengler, J. D., and Raizeene, M. E., 1991, Respiratory health and PM10 pollution: a daily time series analysis.: Am. Rev. Respir. Dis., v. 144, p. 668-674.

Prospero, J. M., Ginoux, P., Torres, O., Nicholson, S. E., and Gill, T. E., 2002, Environmental characterization of global sources of atmospheric dust identified with the Nimbus 7 total ozone mapping spectrometer (TOMS) absorbing aerosol product: Rev. Geophys, v. 40.

Rasoazanamparany, C., Widom, E., Valentine, G. A., Smith, E. I., Cortés, J. A., Kuentz, D., and Johnsen, R., 2015, Origin of chemical and isotopic heterogeneity in a mafic, monogenetic volcanic field: A case study of the Lunar Crater Volcanic Field, Nevada: Chemical Geology, v. 397, p. 76-93.

Reynolds, R. L., Belnap, J., Reheis, M., Lamothe, P., and Luiszer, F., 2001, Aeolian dust in Colorado Plateau soils: Nutrient inputs and recent change in source.: Proc. Natl. Acad. Sci. USA, v. 98, p. 7123–7127.

Salifu, M., Aiglsperger, T., Hällström, L., Martinsson, O., Billström, K., Ingri, J., Dold, B., Alakangas, L. (2018). Strontium (87Sr/86Sr) isotopes: A tracer for geochemical processes in mineralogically-complex mine wastes. Applied Geochemistry, 99, 42-54. ISSN 0883-2927. doi:10.1016/j.apgeochem.2018.10.022.

Steiger, R. H., and Jäger, E., 1977, Subcommission on geochronology: Convention on the use of decay constants in geo- and cosmochronology: Earth and Planetary Science Letters, v. 36, p. 359-362.

Stewart, J. H., and Carlson, J. E., 1978, Geologic Map of Nevada: U.S. Geological Survey and Nevada Bureau of Mines and Geology, 1:500,000: U.S. Geological Survey.

USGS, 1954, Geologic map of Oklahoma: U.S. Department of the Interior.

-, 1979, Geologic map of Colorado: U.S. Department of the Interior.

-, 2003, Geologic map of New Mexico: U.S. Department of the Interior.

Wanquan, T., Honglang, X., Jianjun, Q., Zheng, X., Gensheng, Y., Tao, W., and Xiaoyou, Z., 2004, Measurements of dust deposition in Gansu Province, China, 1986–2000: Geomorphology, v. 57, no. 1-2, p. 41-51.

Webb, N. P., Herrick, J. E., Hugenholtz, C. H., Zobeck, T. M., and Okin, G. S., 2015, Standard Methods for Wind Erosion Research and Model Development: National Wind Erosion Research Network.

Webb, N. P., Herrick, J. E., Van Zee, J. W., Courtright, E. M., Hugenholtz, C. H., Zobeck, T. M., Okin, G. S., Barchyn, T. E., Billings, B. J., Boyd, R., Clingan, S. D., Cooper, B. F., Duniway, M. C., Derner, J. D., Fox, F. A., Havstad, K. M., Heilman, P., LaPlante, V., Ludwig, N. A., Metz, L. J., Nearning, M. A., Norfleet, M. L., Pierrson, F. B., Sanderson, M. A., Sharratt, B. S., Steiner, J. L., Tatarko, J., Tedela, N. H., Toledo, D., Unnasch, R. S., Van Pelt, S., and Wagner, L., 2016, The National Wind Erosion Research Network: Building a standardized long-term data resource for aeolian research, modeling and land management: Aeolian Research, v. 22, p. 23-36.

Xu, X., Levy, J. K., Zhaohui, L., and Hong, C., 2006, An investigation of sand–dust storm events and land surface characteristics in China using NOAA NDVI data: Global and Planetary Change, v. 52, no. 1, p. 182-196.

Zeng, W., Wan, X., Wang, L., Lei, M., Chen, T., and Gu, G., 2022, Apportionment and location of heavy metal(loid)s pollution sources for soil and dust using the combination of principal component analysis, Geodetector, and multiple linear regression of distance: Journal of Hazardous Materials, v. 438, p. 129468.

Zhang, J., 1994, Atmospheric wet deposition of nutrient elements: correlation with harmful biological blooms in Northwest Pacific Coastal Zones: Ambio, v. 23, p. 464-468.

Zhao, W., Sun, Y., Balsam, W., Zeng, H., Lu, K., Otgonbayar, K., and Ji, J., 2015, Clay-sized Hf-Nd-Sr isotopic composition of mongolian dust as a fingerprint for regional to hemispherical transport: Geophys. Res. Lett.

8. FIGURES

Figure 1. Map of NWERN sites across the western United States with $^{87}Sr/^{86}Sr$ ratios.

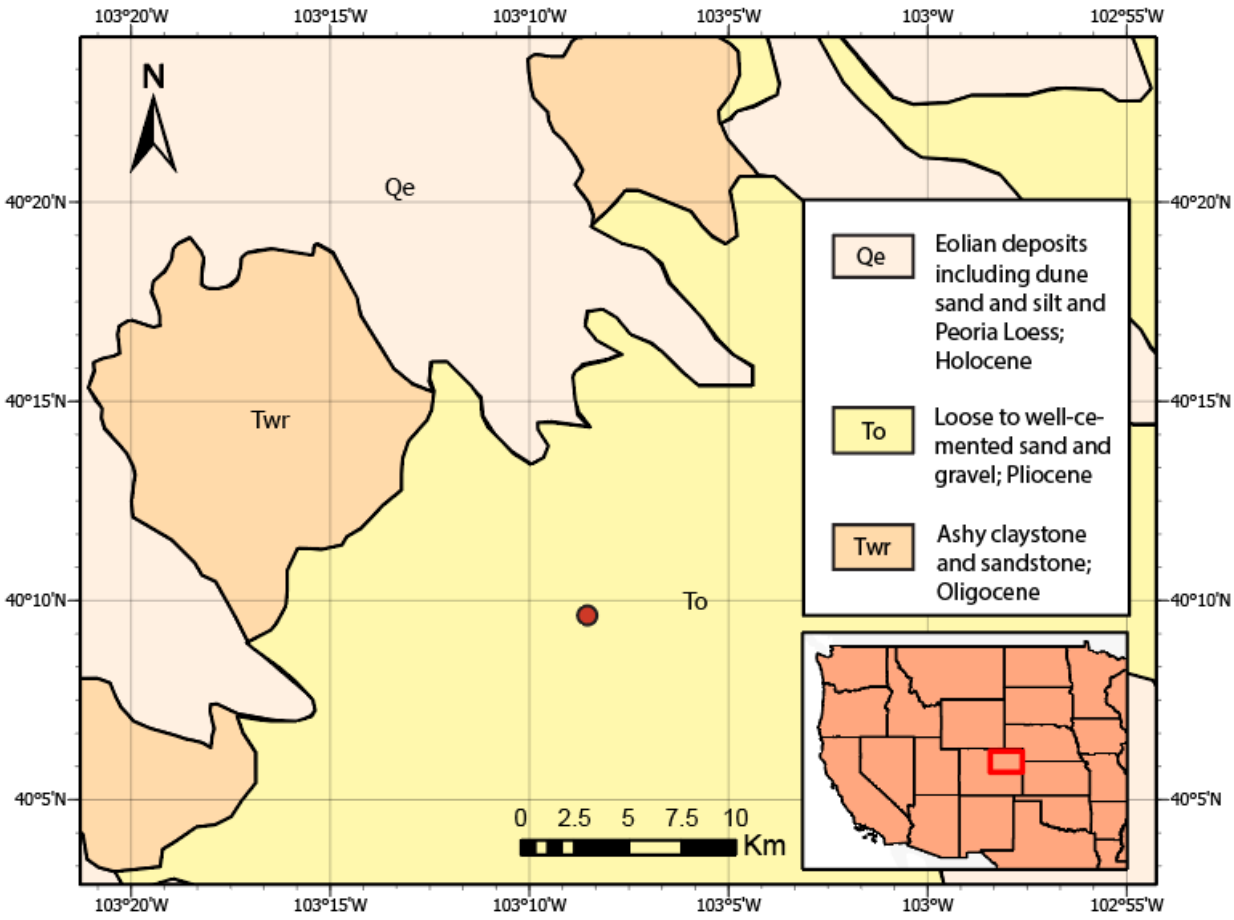

Figure 2. Geologic map of Akron, CO Modified from the Geologic Map of Colorado produced by the U.S. Geological Survey in 1979. Area consists of loose to well-cemented sand and gravels in the Ogallala Formation (To), ashy claystone, sandstones, and conglomerate units in the White River Formation (Twr), Quaternary aged alluvium, gravels, and eolian deposits (Qe).

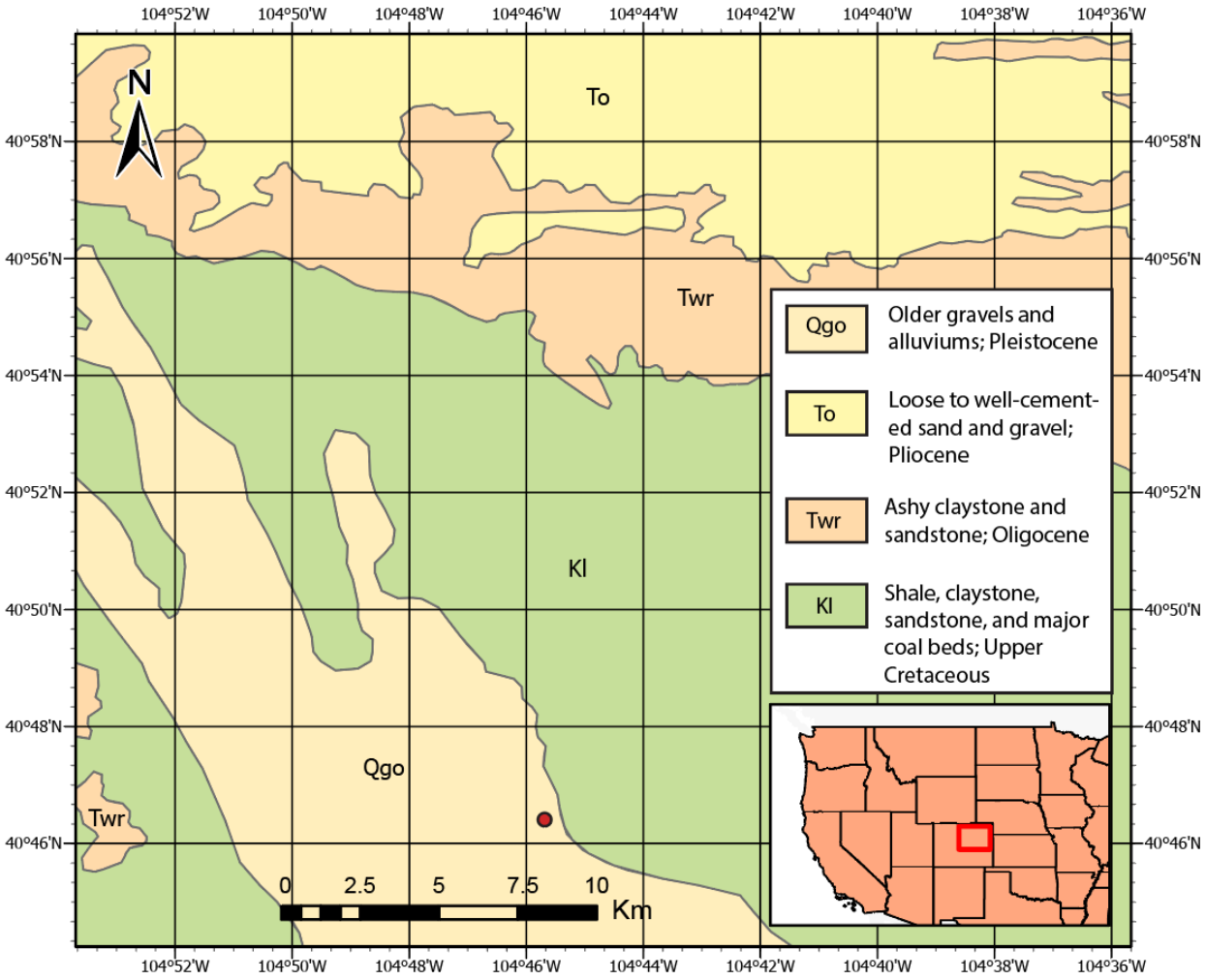

Figure 3. Geologic map of the Central Plains Experimental Range (CPER), CO . Modified from the Geologic Map of Colorado produced by the U.S. Geological Survey in 1979. Area consists of shale, claystone, and sandstone from the Laramie Formation (Kl) and the Fox Hills Sandstone to the south. Surrounding area consists of loose to well-cemented sands and gravels in the Ogallala Formation (To), ashy claystone, sandstones, and conglomerate units in the White River Formation (Twr), and Quaternary aged alluvium, gravels, and eolian deposits (Ogo).

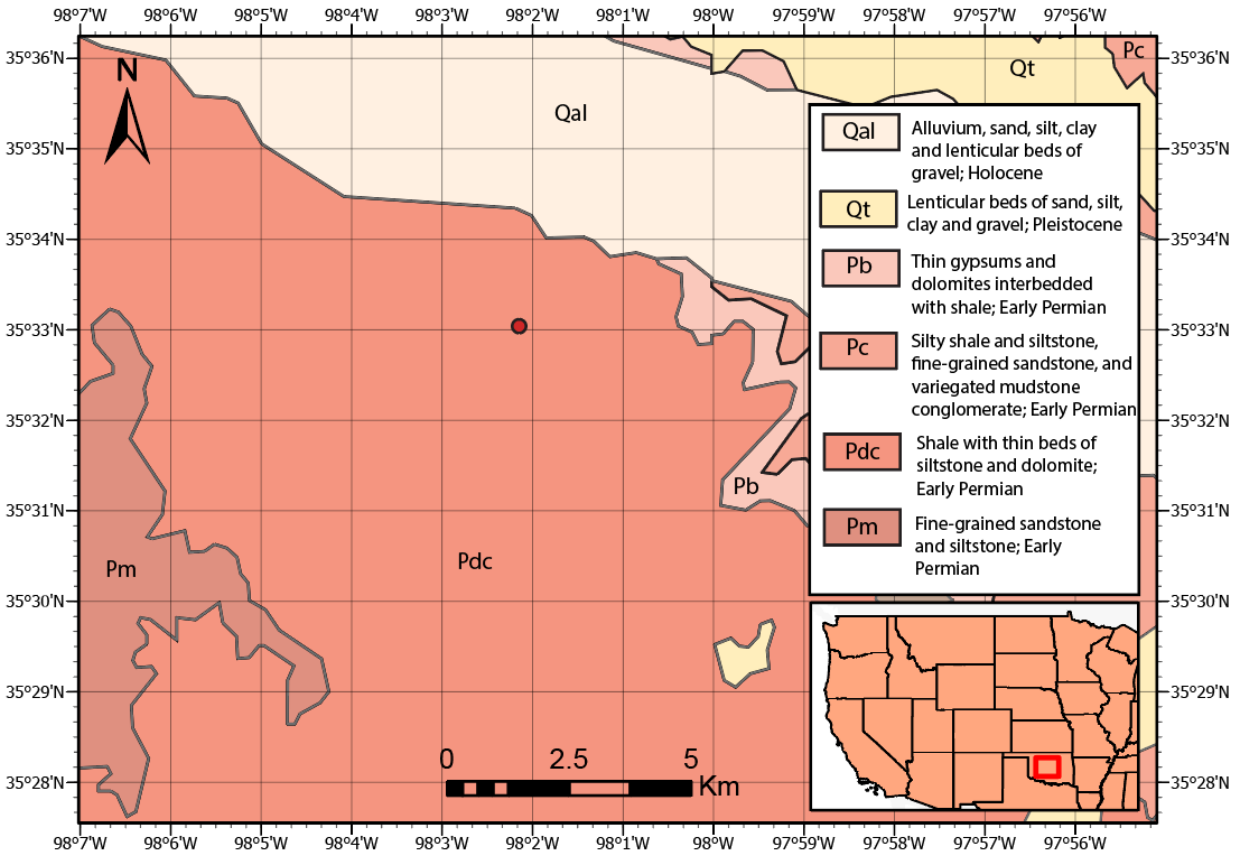

Figure 4. Geologic map of El Reno, OK . Modified from the Geologic Map of Oklahoma produced by the U.S. Geological Survey in 1954. Area consists of Permian aged shale with layers of siltstone and dolomite (Pdc). Surrounding area consists of Permian aged sandstone, gypsum, and dolomite (Pm, Pc) with Pleistocene clays and gravels (Qt) and Holocene alluvium (Qal).

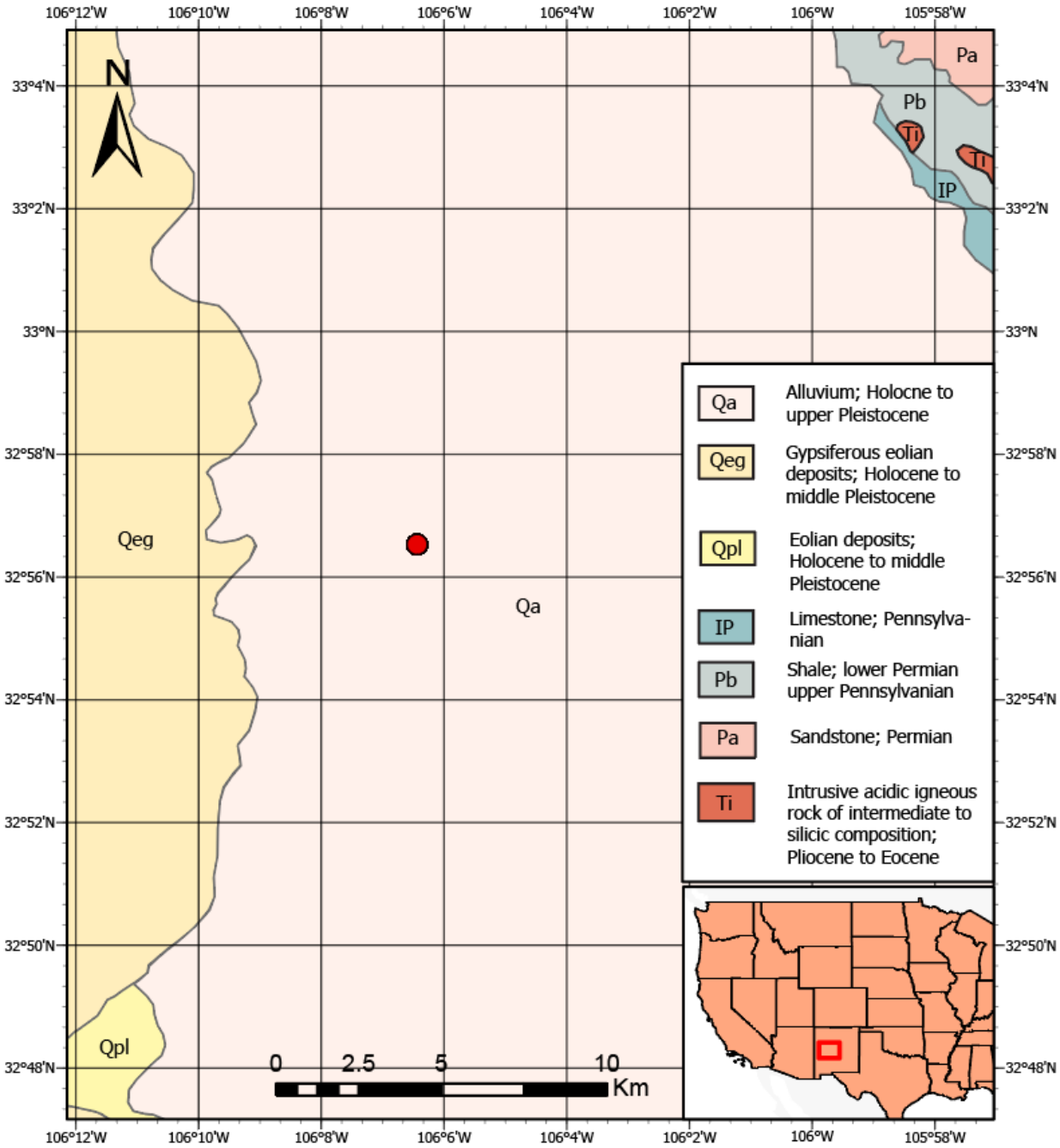

Figure 5. Geologic map of HAFB, NM . Modified from the Geologic map of New Mexico produced by the U.S. Geological Survey in 2003. The site consists of Quaternary eolian (Qe), gypsiferous eolian from White Sands National Park (Qeg), and alluvium (Qa) with limestones (IP), shales (Pb) and intermediate to silicic volcanic rocks (Ti) nearby. This area is enclosed on either side by the Sacramento and San Andres mountains.

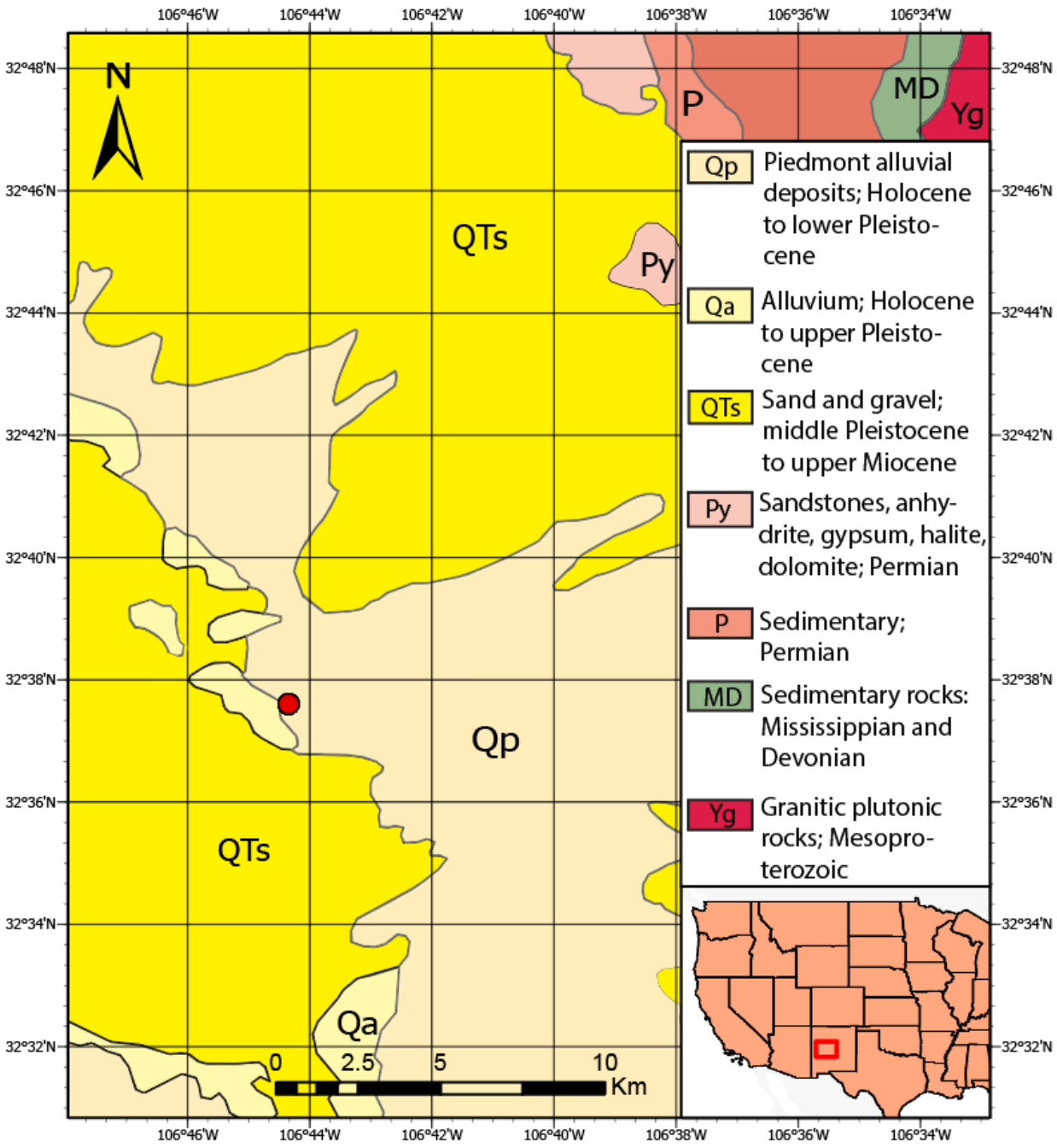

Figure 6. Geologic map of Jornada, NM . Modified from the Geologic map of New Mexico produced by the U.S. Geological Survey in 2003. This site consists of Quaternary piedmont alluvium (Qp, Qa) and is surrounded by Quaternary sands and gravels (QTs), Permian sandstones, limestones, gypsums, halite, and dolomite (Py, P, Ph), granitic plutonic rocks (Yg), and mafic metavolcanic rocks (Xvm).

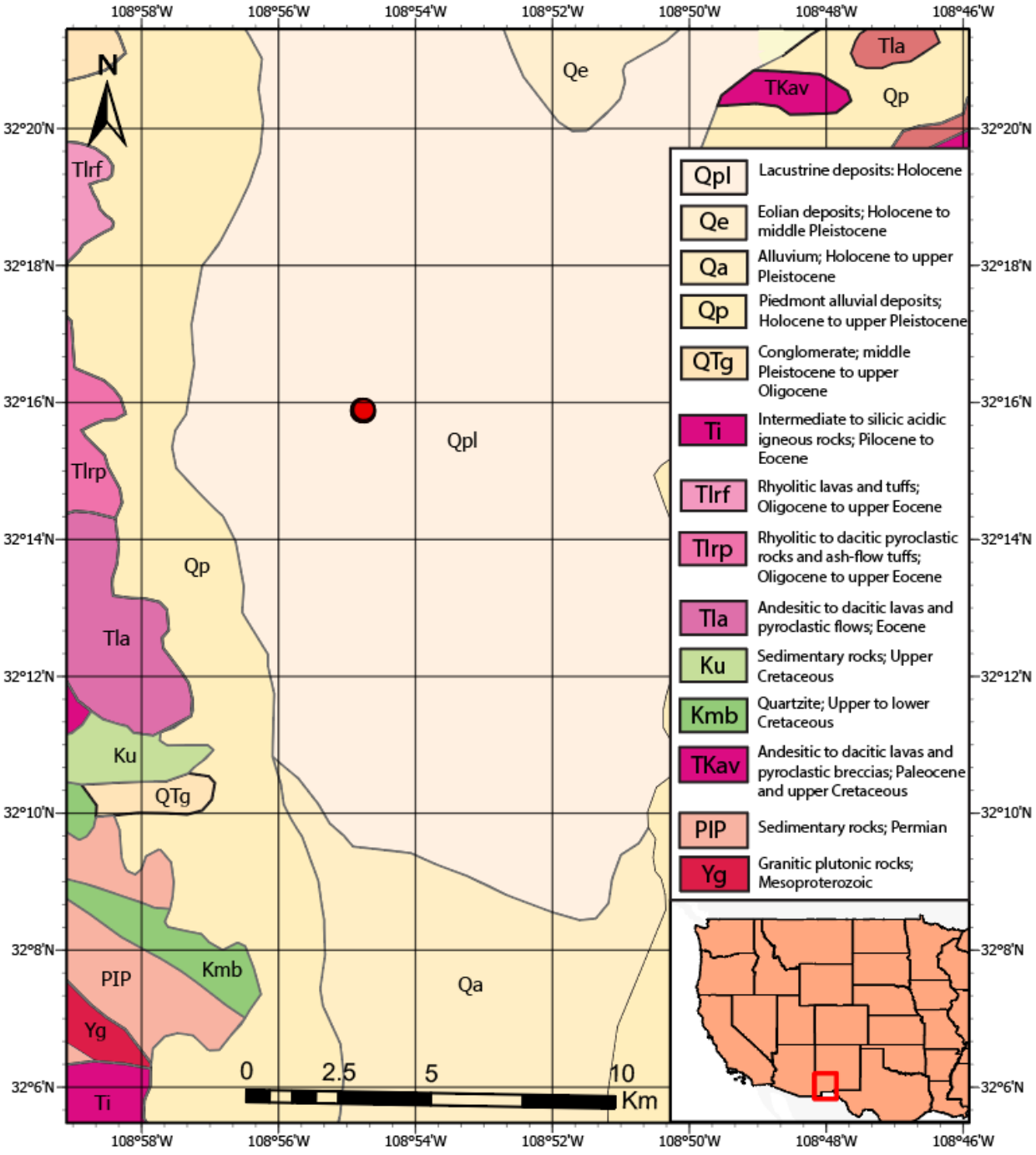

Figure 7. Geologic map of Lordsburg, NM . Modified from the Geologic map of New Mexico produced by the U.S. Geological Survey in 2003. This site consists of lacustrine playa deposits (Qpl) and is surrounded by piedmont alluvium (Qp, Qa), silicic volcanic rocks (Tl, Tlrf, Tlrp, Tlv, Tla, Tkav), quartzite (Kmb), and sedimentary rocks (Ku, PIP).

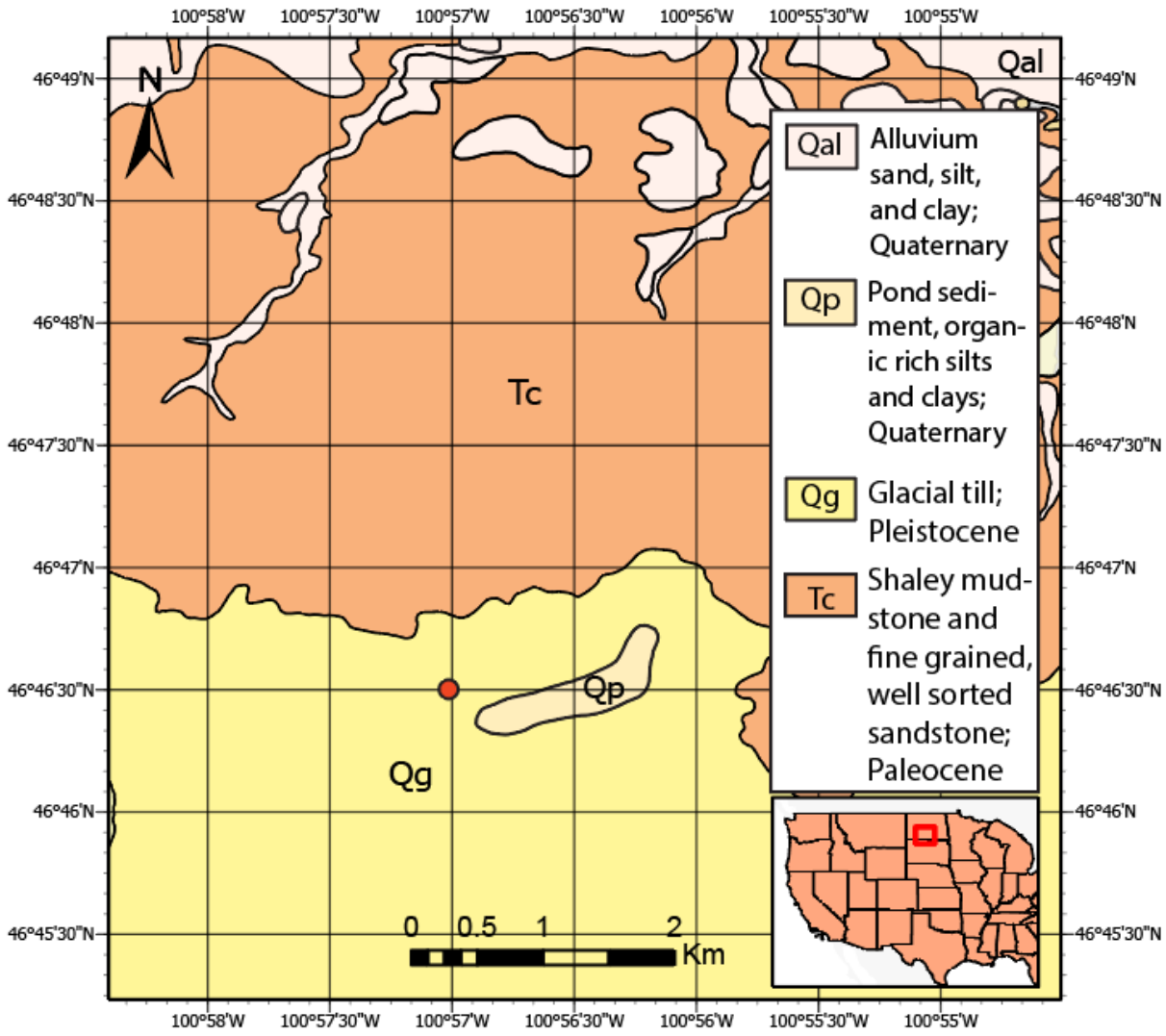

Figure 8. Geologic map of Mandan, ND . Modified from the Surface Geology Mandan Quadrangle produced by the North Dakota Geological Survey in 1999. This site sits on Pleistocene glacial till (Qp), surrounded by shaley mudstone (Tc), organic rich pond sediments (Qp), and alluvium (Qal, Qat).

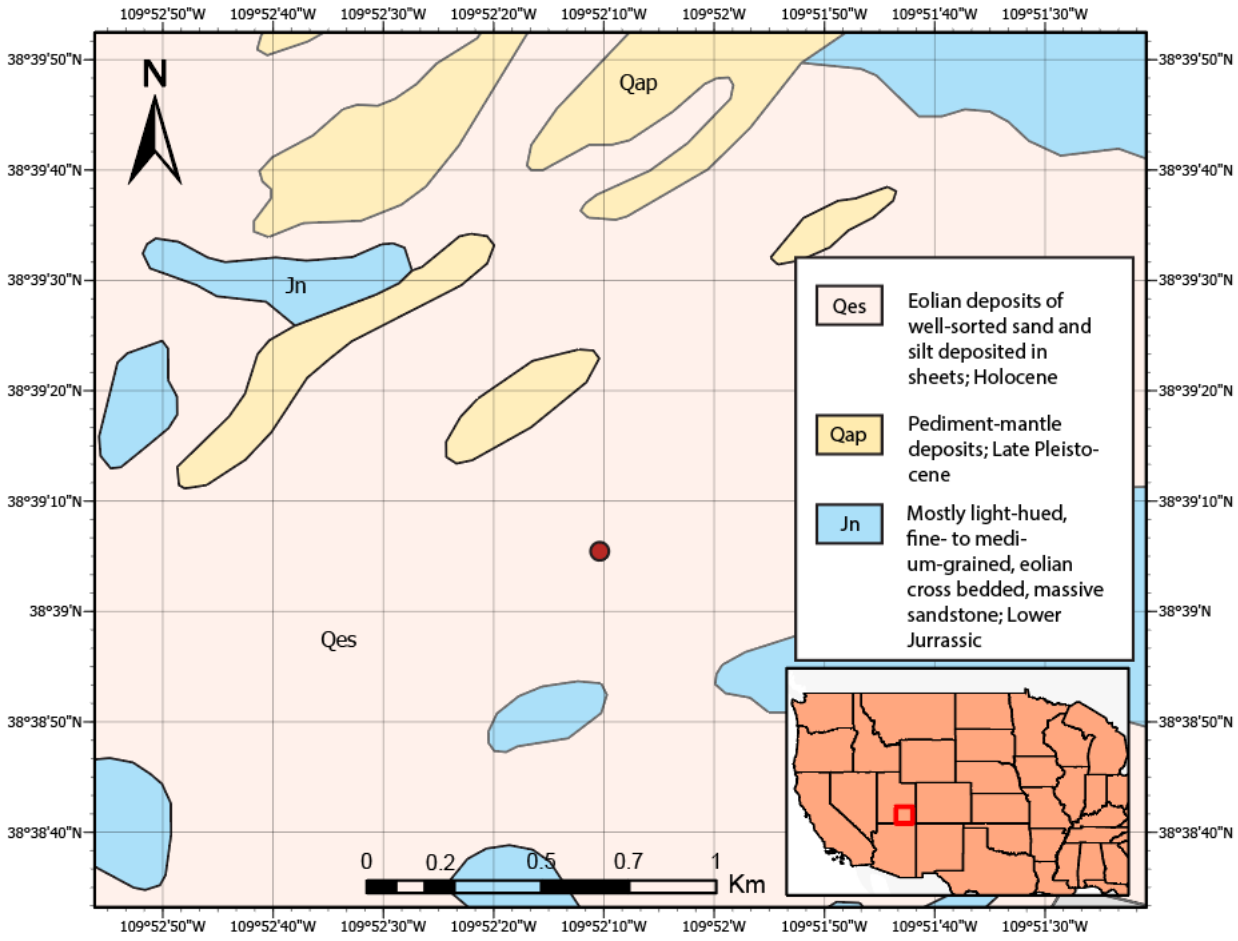

Figure 9. Geologic map of Moab, UT . Modified from the Geologic map of the Moab and Eastern part of the San Rafael desert produced by the Utah Geological Survey in 2002. This site is located on eolian sand deposits (Qes) and surrounded by pediment-mantle deposits (Qap) and sandstone (Jn).

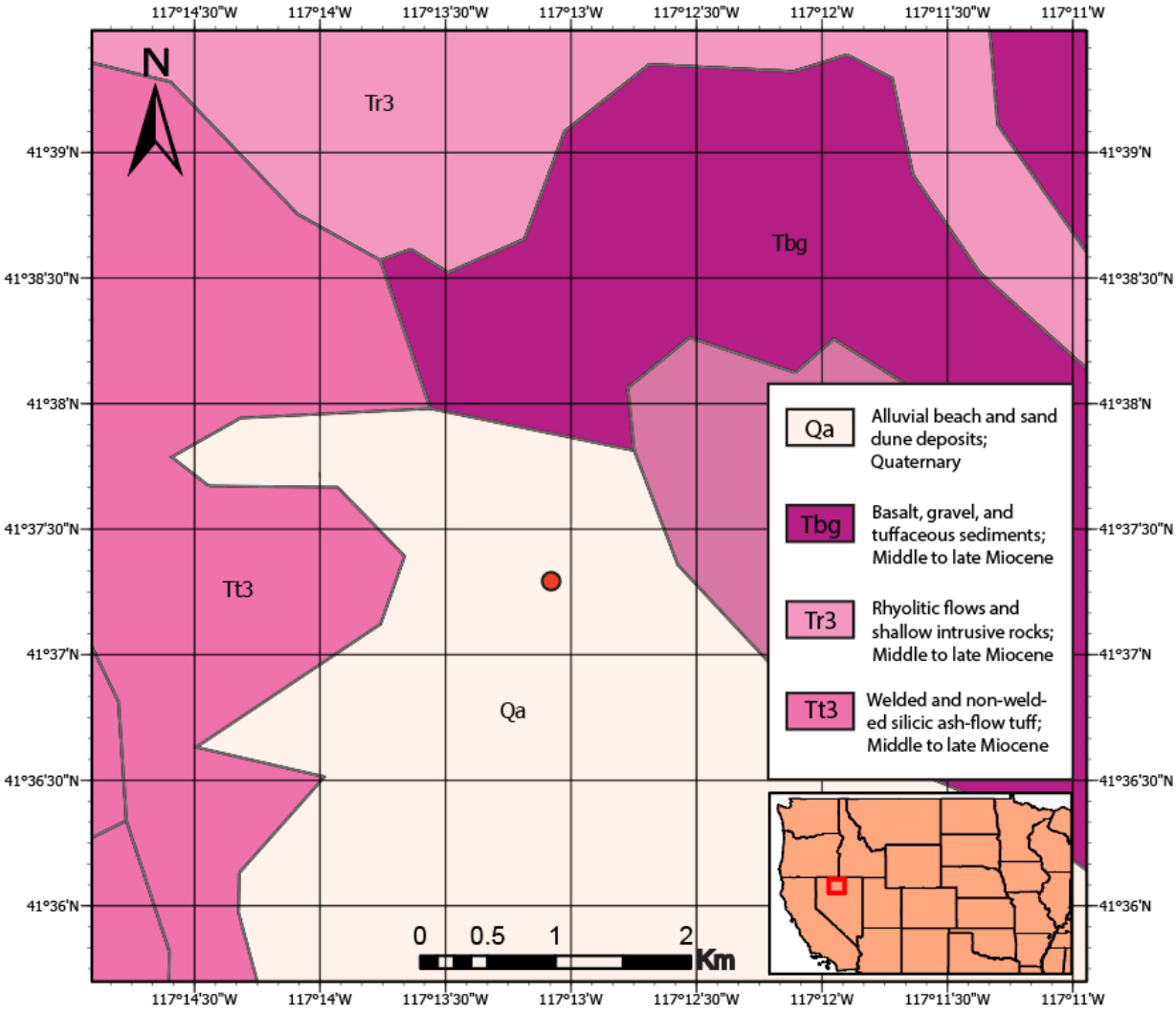

Figure 10. Geologic map of Red Hills, NV . Modified from the Geologic map of Nevada produced by the U.S. Geological Survey in 1981. This site is located on alluvial beach and sand dune deposits (Qa) surrounded by basalts (Tbg), rhyolitic flows (Tr3), and silicic ash-flow tuffs (Tt3).

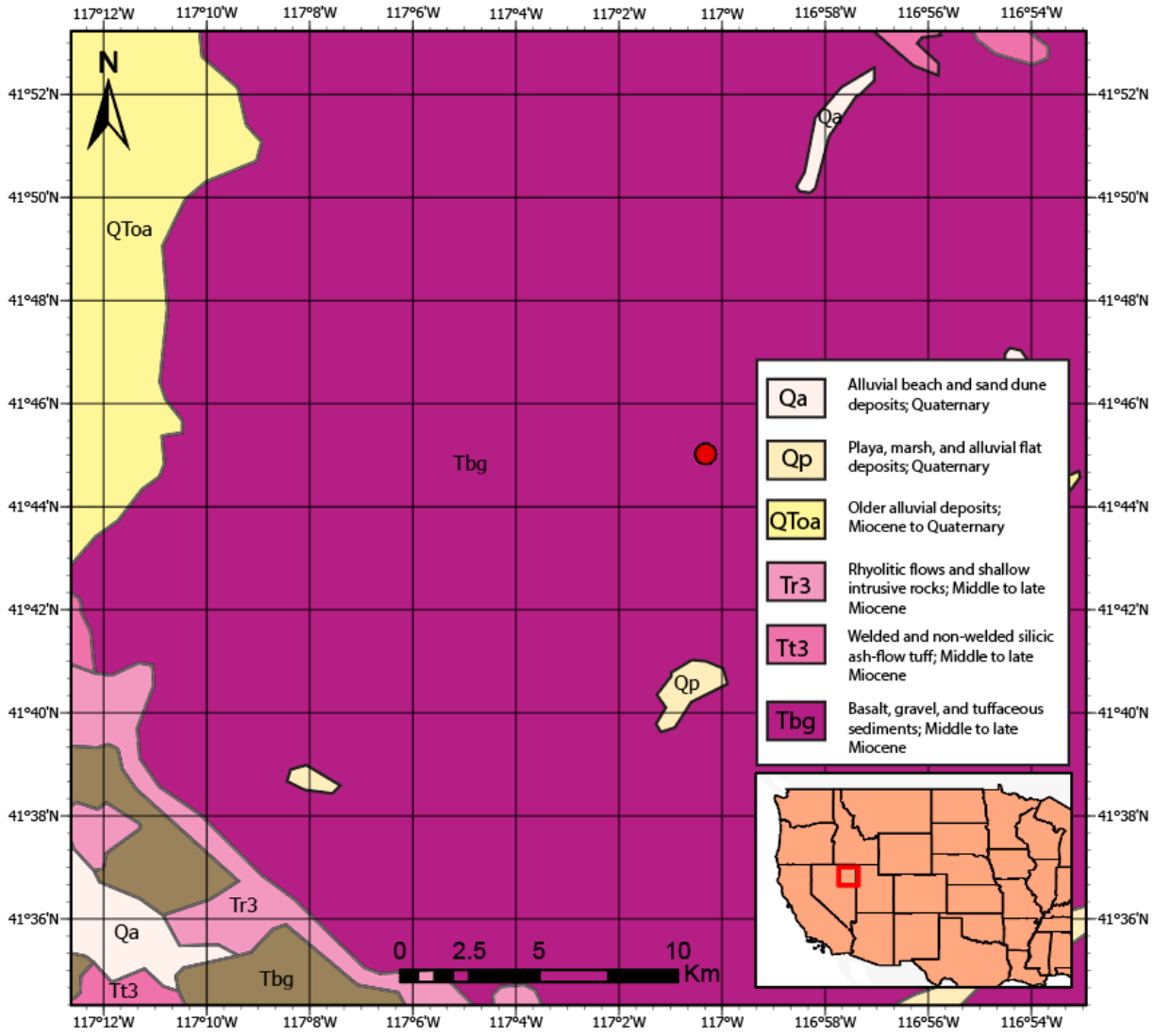

Figure 11. Geologic map of Twin Valley, NV . Modified from the Geologic map of Nevada produced by the U.S. Geological Survey in 1981. This site is located on basalt (Tbg), surrounded by playa (Qp), alluvial beach and sand dunes (Qa), rhyolitic flows (Tt3), and silicic ash-flow tuffs (Tt3).

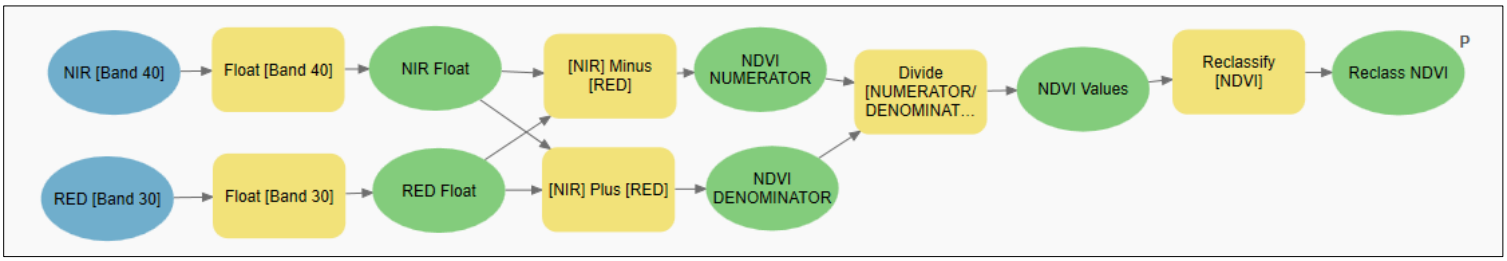

Figure 12. Model Builder used to calculate NDVI for each Landsat 8 image.

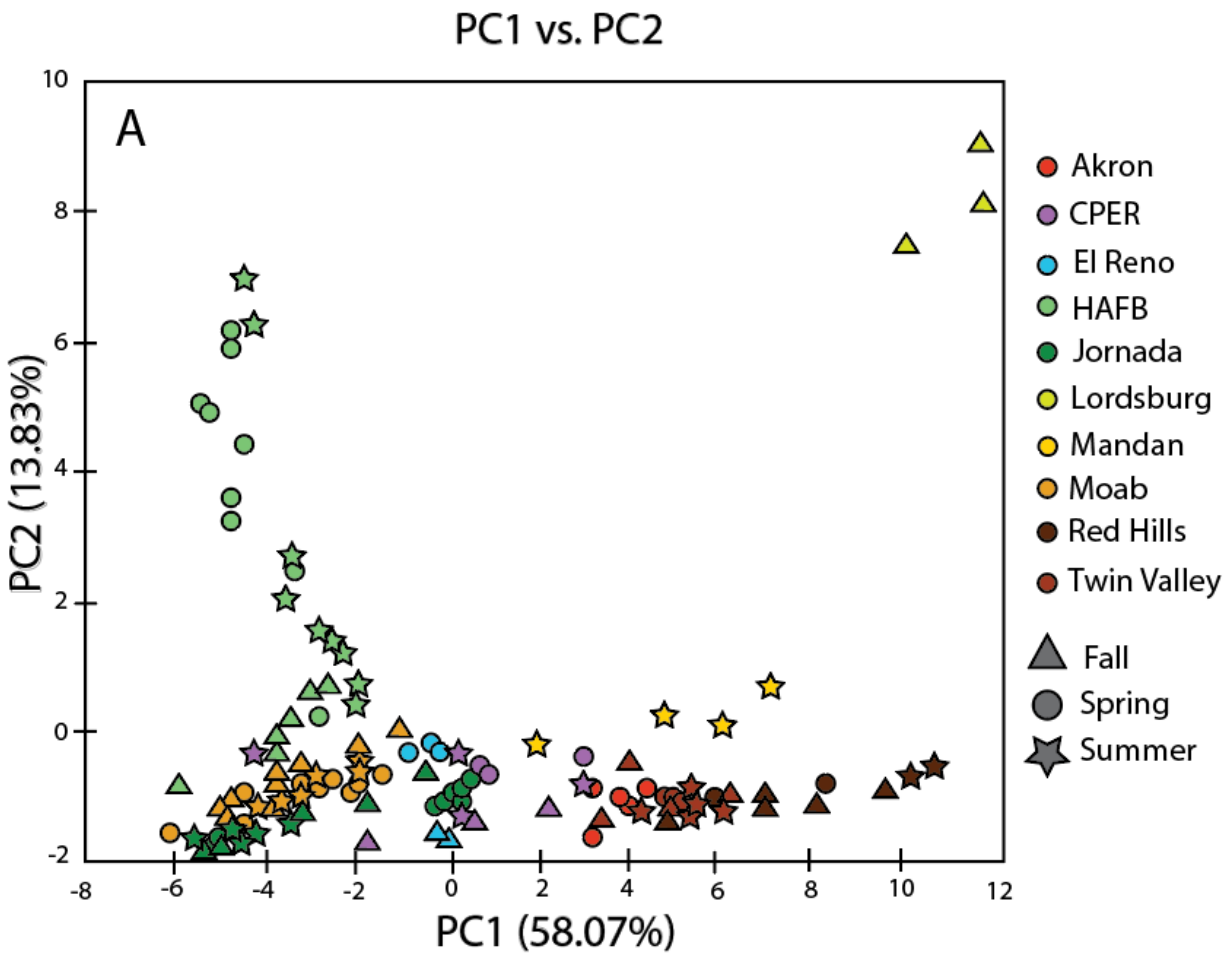
PC1 vs. PC2
A
PC2 (13.83%)
PC1 (58.07%)
10
8
6
4
2
0
-2
-8
-6
-4
-2
0
2
4
6
8
10
12
Akron
CPER
El Reno
HAFB
Jornada
Lordsburg
Mandan
Moab
Red Hills
Twin Valley
Fall
Spring
Summer

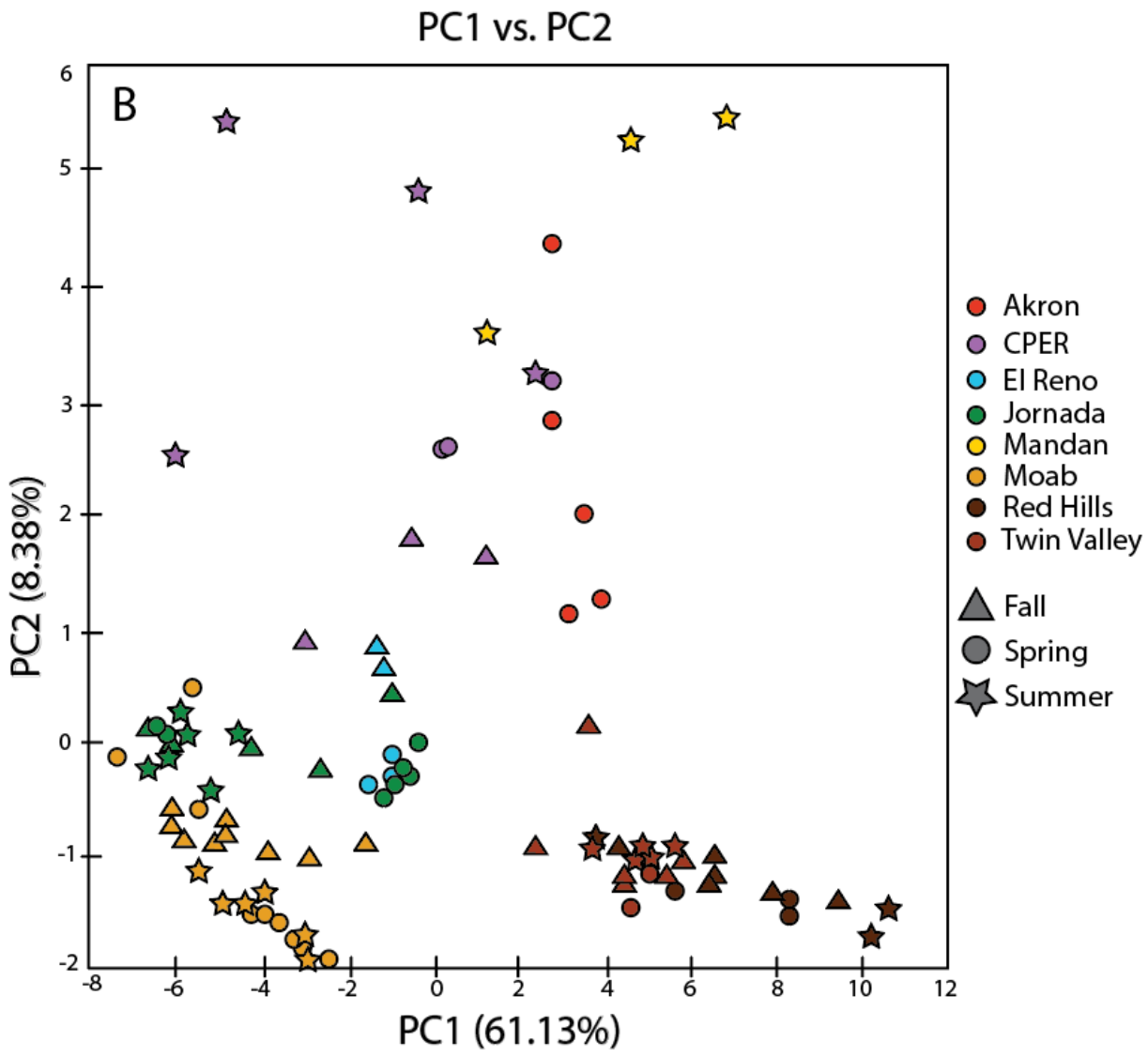
PC1 vs. PC2
B
PC2 (8.38%)
PC1 (61.13%)
6
5
4
3
2
1
0
-1
-2
-8
-6
-4
-2
0
2
4
6
8
10
12
Akron
CPER
El Reno
Jornada
Mandan
Moab
Red Hills
Twin Valley
Fall
Spring
Summer

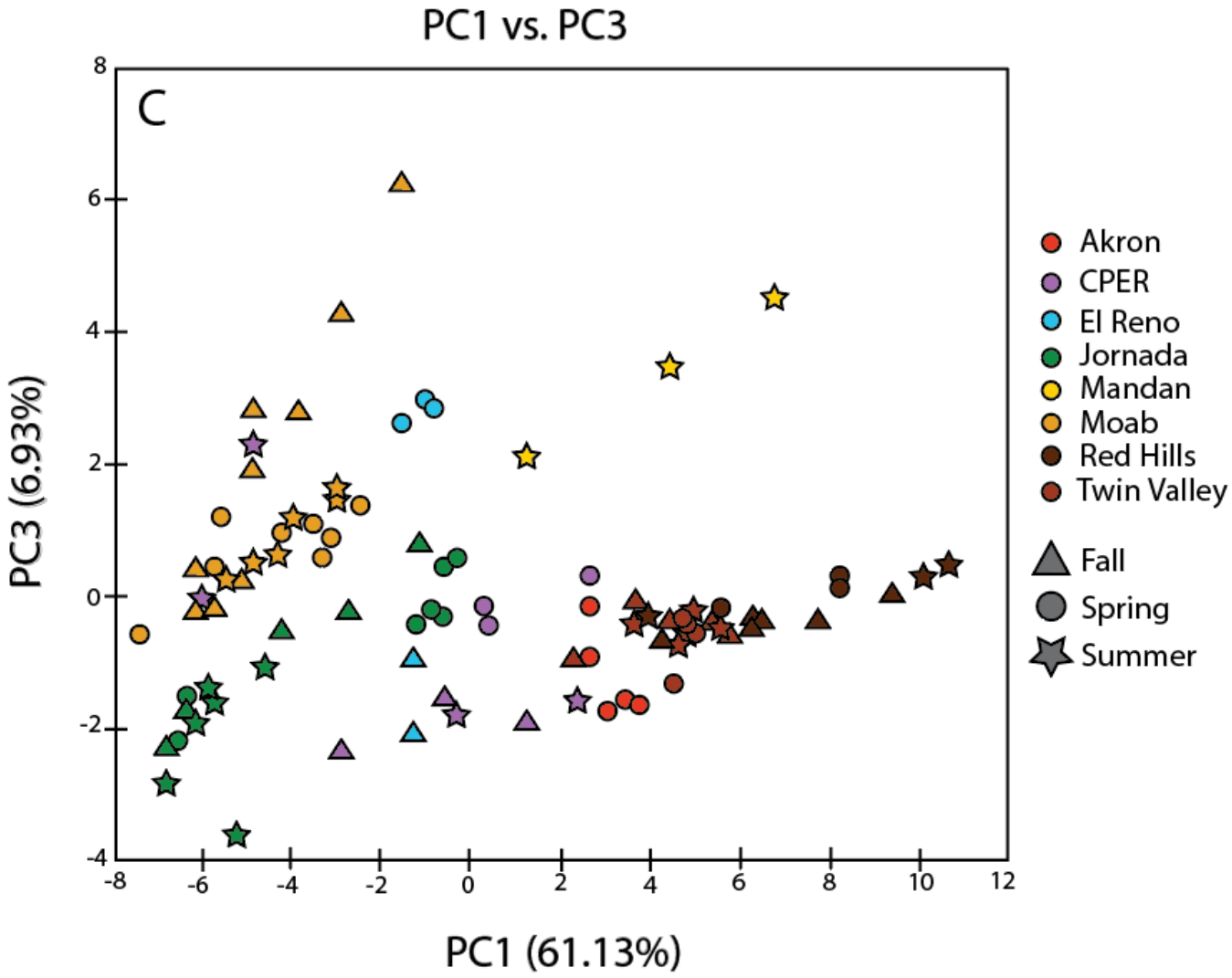

Figure 13. Principal component analysis (PCA) for 40+ trace and major elements analyzed in all the NWERN samples and seasons. A) PCA run with all NWERN sites for PC1 (Be, Al, Ka, Sc, Fe, Rb, As, Cs, REE+Y) vs PC2 (Li, Na, Mg, Ca, Cr, Cu, Se, Sr, Mo). B) PCA run without HAFB and Lordsburg sites for PC1 (Li, Be, K, Sc, V, Mn, Fe, Co, Rb, As, REE+Y) vs PC2 (Cr, Ni, Se, Mo, Cd, Tl, Pb) C) PCA run without HAFB and Lordsburg sites for PC1 (Li, Be, K, Sc, V, Mn, Fe, Co, Rb, As, REE+Y) vs PC3 (Na, Mg, Al, Ca, Cu, Sr, -Sb).

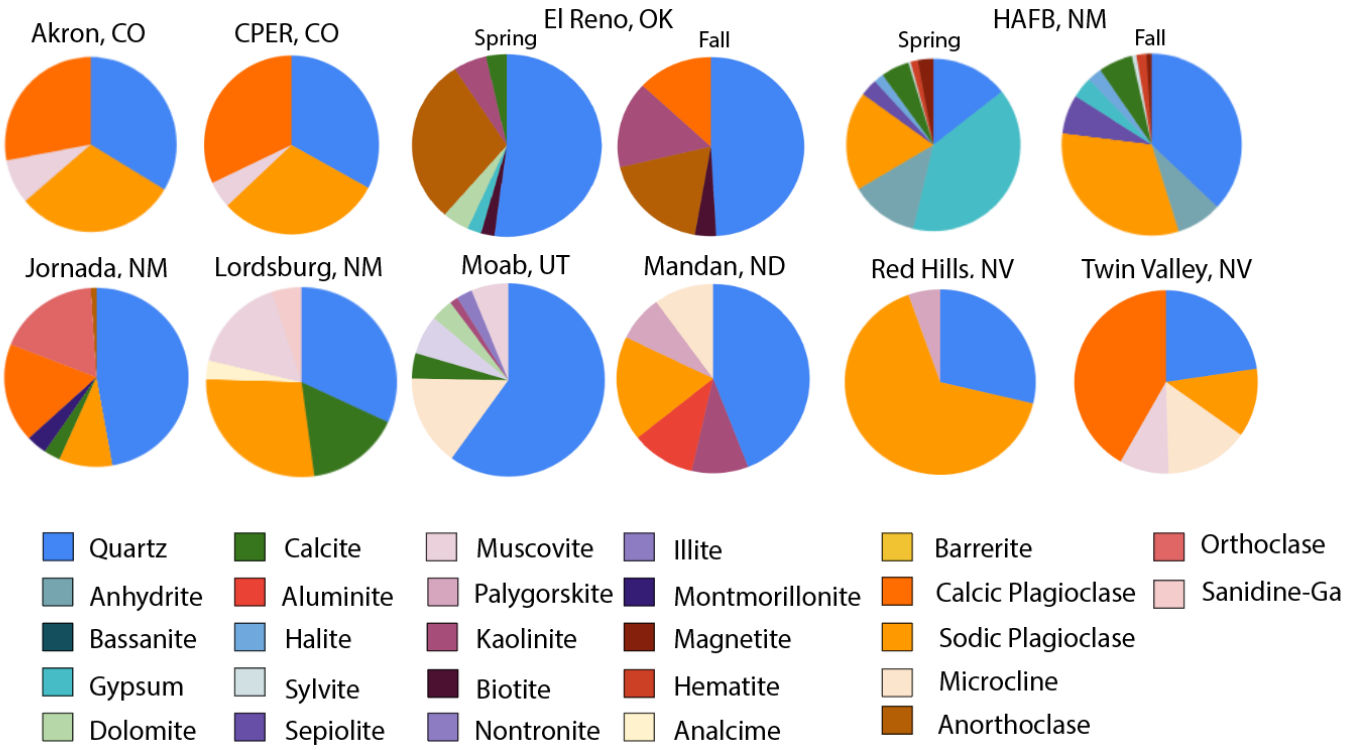

Figure 14. Averaged XRD results for each NWERN site . El Reno, OK and HAFB, NM showed seasonal variation in their mineralogy, which is labeled as 'spring' and 'fall.'

Mineralogy			Akron	CPER	El Reno		HAFB		Jornada	Lordsburg	Moab	Mandan	Red Hills	Twin Valley
					Sp	Fa	Sp	Fa						
Quartz	SiO2	Silica Dioxide	✓	✓	✓	✓	✓	✓	✓	✓	✓	✓	✓	✓
Anhydrite	CaSO4	Calcium Sulfate					✓	✓						
Bassanite	2CaSO4 · H2O	Calcium Sulfate					✓	✓						
Gypsum	CaSO4 · 2H2O	Calcium Sulfate			✓		✓	✓						
Dolomite	CaMg(CO3)2	Carbonate			✓						✓			
Calcite	CaCO3	Carbonate			✓		✓	✓	✓	✓	✓			
Aluminite	Al2SO4(OH)4 · 7H2O	Aluminum Sulfate										✓		
Halite	NaCl	Sodium Chloride					✓	✓						
Sylvite	KCl	Potassium Chloride					✓	✓						
Sepiolite	Mg4Si6O15(OH)2 · 6H2O	Magnesium Silicate					✓	✓						
Muscovite	KAl2(AlSi3O10)(F, OH)2	Phyllosilicate	✓	✓					✓	✓				✓
Palygorskite	(Mg, Al)2Si4O10(OH) · 4H20	Phyllosilicate									✓	✓		
Kaolinite	Al2(OH)4Si2O5	Phyllosilicate			✓	✓				✓	✓			
Biotite	K(Mg, Fe)3(AlSi3O10)(F, OH)2	Phyllosilicate			✓	✓								
Nontronite	(CaO0.5,Na)0.3Fe3+2(Si,Al)4O10(OH)2·nH2O	Phyllosilicate								✓				
Illite	(K, H3O)(Al, Mg, Fe)2(Si, Al)4O10[(OH)2, (H2O)]	Phyllosilicate								✓				
Montmorillonite	(Na, Ca)0.33(Al, Mg)2(Si4O10)(OH)2 · nH2O)	Phyllosilicate					✓							
Magnetite	Fe2+Fe3+2O3	Iron Oxide				✓	✓							
Hematite	Fe2O3	Iron Oxide				✓	✓							
Analcime	NaAlSi2O6 · H2O	Zeolite							✓					
Anorthite	CaAl2Si2O8	Feldspar	✓	✓	✓			✓						✓
Albite	NaAlSi3O8	Feldspar		✓		✓	✓	✓	✓		✓	✓	✓	✓
Microcline	KAlSi2O8	Feldspar			✓	✓				✓	✓			✓
Anorthoclase	(Na,K)AlSi3O8	Feldspar						✓						
Orthoclase	KAlSi3O8	Feldspar						✓						
Sanidine-Ga	K(AlSi3O8)	Feldspar							✓					

Figure 15. Mineral composition for each NWERN site

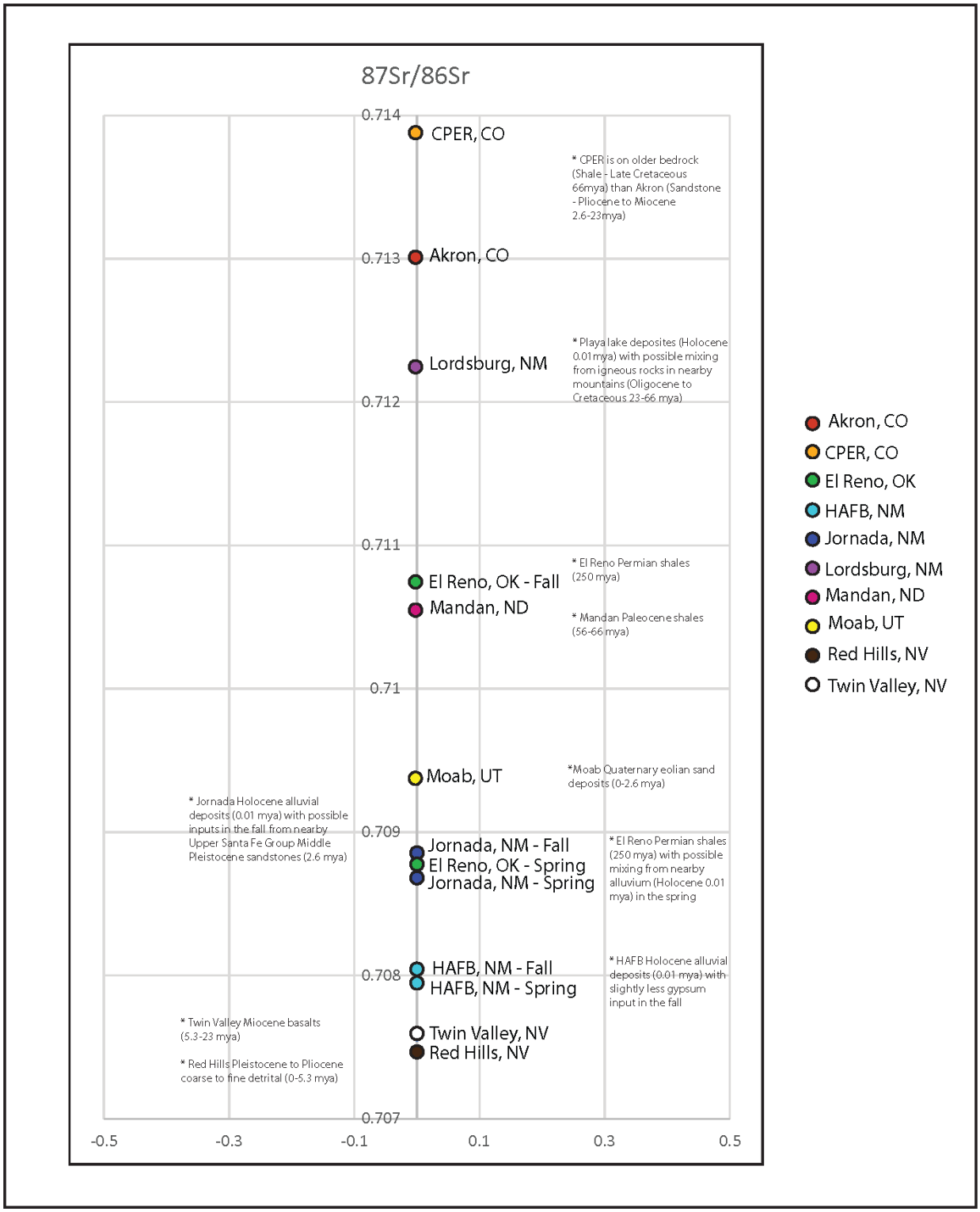

Figure 16. Strontium isotope ($^{87}Sr/^{86}Sr$) ratios for dust collected by NWERN in the western United States.

9. TABLES

Table 1. Basic characteristics of each NWERN site

Location	State	Avg Rainfall (mm)	Elevation (m)	Soil Texture	Land Type	Number of Samples
Akron	Colorado	421	1383	Silty Loam	Agriculture	6
CPER	Colorado	320	1650	Sandy Loam	Grazed	11
El Reno	Oklahoma	815	420	Silt Loam	Agriculture	5
HAFB	New Mexico	278	1267	Silt Loam/Sandy Loam	Grazed	24
Jornada	New Mexico	250	1320	Sandy Loam/Silt Loam	Grazed	20
Lordsburg	New Mexico	286	1267	Silt Loam	Playa	2
Mandan	North Dakota	410	591	Silt Loam	Agriculture	3
Moab	Utah	229	1575	Sandy Loam	Grazed	24
Red Hills	Nevada	200	1725	Silt Loam	Grazed	12
Twin Valley	Nevada	200	1668	Silt Loam	Grazed	15